JAAS
Journal of Analytical Atomic Spectrometry

Accepted Manuscript

This article can be cited before page numbers have been issued, to do this please use: S. Bhattacharjee, J. Wostbrock, C. Blättler, T. Present, M. G. Sliwinski, Y. Guan and D. S. Grewal, *J. Anal. At. Spectrom.*, 2026, DOI: 10.1039/D6JA00136J.

ROYAL SOCIETY OF CHEMISTRY

rsc.li/jaas

View Article Online
DOI: 10.1039/D6JA00136J

Accurate *in situ* C-Mg-Ca isotope ratio analysis in carbonates using SIMS

Surjyendu Bhattacharjee[1]*, Jordan A.G. Wostbrock[1], Clara L. Blättler[2], Ted Present[3], Maciej G. Sliwinski[4], Yunbin Guan[3] and Damanveer S. Grewal[1]*

[1]Department of Earth & Planetary Sciences, Yale University, New Haven, CT 06511, USA
[2]Department of the Geophysical Sciences, University of Chicago, Chicago, IL 60637, USA
[3]Division of Geological and Planetary Sciences, California Institute of Technology, Pasadena, CA 91125, USA
[4]Department of Geosciences, University of Alaska, Fairbanks, AK 99775, USA

*correspondence: surjyendu.bhattacharjee@yale.edu, damanveer.grewal@yale.edu

Abstract

Isotopic compositions of carbonate-forming elements (C, O, Mg, Ca) are widely used geological proxies. Non-traditional stable isotope ratios (Mg, Ca) of carbonates can constrain water-rock reactions and precipitation kinetics but are typically measured by bulk digestion techniques that lack textural context and can be contaminated by elements released from associated phases (e.g., phyllosilicates). This is particularly problematic for micron-scale, chemically zoned extraterrestrial carbonates from asteroid-returned samples, carbonaceous chondrites, and Martian meteorites. Secondary ion mass spectrometry (SIMS) provides a reliable *in situ* approach, but its application to Mg and Ca isotopes in carbonates has been limited by the lack of well-characterized standards spanning the dolomite-ankerite and magnesite-siderite solid-solution series. Here we present 22 carbonate standards (10 dolomite-ankerite, 11 magnesite-siderite, and 1 calcite) for coupled C-Mg-Ca isotope analysis at 10-20 µm spatial resolution using a Cameca IMS 7f-GEO ion microprobe. The instrumental mass fractionation (IMF) for each isotopic system varies non-linearly with Fe+Mn content of carbonates, parameterized as (Fe+Mn)# [= molar (Fe+Mn)/(Fe+Mn+Mg)], and is modelled using polynomial or sigmoidal functions ($R^2 \geq 0.92$) with calibration residuals ≤0.7‰ (1SD). Application of these calibrations to compositionally zoned secondary standards yields grain-averaged isotopic compositions that agree with independent bulk measurements within propagated 2SE uncertainties, validating the accuracy of the protocol at per-mille-level precision. This work enables accurate, texture-resolved coupled C-Mg-Ca isotopic microanalysis of complex terrestrial and extraterrestrial carbonates.

Introduction

Isotopic compositions of carbon, oxygen, and non-traditional stable elements (Mg, Ca) in carbonates archive the environments in which they precipitate, serving as versatile proxies for terrestrial and extraterrestrial processes[1–3]. Traditional C-O isotope ratios and ^{13}C-^{18}O "clumped" isotopic compositions track the nature and source of the carbonate forming fluids, fluid evolution, and temperatures of carbonate formation[4–10]. Non-traditional stable isotopic compositions (Mg, Ca) can additionally constrain water-rock reactions[11–13], elemental cycling[14], and precipitation kinetics[15–17]. These measurements are typically obtained by bulk digestion, which averages multiple carbonate generations, lacks textural context, and is susceptible to contamination from co-existing phases such as phyllosilicates[18,19]. Bulk techniques are particularly poorly suited for

View Article Online
DOI: 10.1039/D6JA00136J

extraterrestrial carbonates, which are typically tens to hundreds of microns in size, often chemically zoned, and intimately associated with phyllosilicates[20]. Examples include the Ca-Mg-Fe zoned carbonate concretions in Martian meteorite ALH84001[21,22] and the diverse carbonate generations in carbonaceous chondrites and asteroid-returned samples (Ryugu[23] and Bennu[24]), which are occasionally Mg-Fe-Mn zoned (**Fig. 1**). For such samples, *in situ* isotopic analysis that preserves textural context is essential and is the only way to avoid the contamination inherent in bulk digestion.

Secondary ion mass spectrometry (SIMS) enables highly precise *in situ* isotope ratio measurements at micrometer spatial resolution[25–27]. Measured isotope ratios differ from the true composition due to instrumental mass fractionation (IMF)[28–34], which arises from differential fractionation during ion sputtering, transmission, and detection[35–37]. IMF is empirically corrected using matrix-matched standards analyzed within the same session[27]. For minerals exhibiting solid solution, IMF varies systematically with chemical composition (the "matrix effect") and must be calibrated across the compositional range of interest.

Carbonate minerals from the dolomite-ankerite and magnesite-siderite solid-solution series are common in terrestrial and extraterrestrial environments[38–40]. For C and O isotopes, SIMS matrix-effect calibrations across these solid solutions are well established, enabling routine *in situ* C-O isotopic analysis of intermediate-composition carbonates[21,41,42,30,43–45,33,34]. However, no analogous calibrations exist for Mg or Ca isotopes across these solid-solution series. Although a previous study has explored Ca isotope analysis in end-member calcite[46] using SIMS, the Mg-Ca isotope microanalysis of intermediate-composition carbonates from the dolomite-ankerite and magnesite-siderite series remains unexplored, largely due to the lack of well-characterized standards spanning these solid solutions. This limitation prevents coupled, texture-resolved non-traditional stable isotope analysis of the chemically complex carbonates that are common in extraterrestrial settings.

Here, we report the development of a suite of dolomite-ankerite, magnesite-siderite, and calcite reference materials for SIMS C-Mg-Ca isotope analysis using a Cameca IMS 7f-GEO at Caltech. We characterize the variation of IMF with major cation chemistry, parameterized as (Fe+Mn)# [= molar (Fe+Mn)/(Fe+Mn+Mg)], across multiple analytical sessions and grain mounts. We demonstrate the accuracy of our calibrations by analyzing chemically zoned carbonate minerals with known C-Mg-Ca isotopic compositions, which closely represent the chemical complexity of natural analytes. This work enables future measurements of coupled C-Mg-Ca isotopic compositions of extraterrestrial carbonates from meteorites and samples returned from asteroids such as Ryugu and Bennu, which is the central motivation of this study.

Materials and methods

Reference materials

Natural Ca-Mg-Fe carbonates were acquired from GPS Division Mineral Collection, California Institute of Technology. Their mineralogy was confirmed by scanning electron microscopy with energy-dispersive X-ray spectroscopy (SEM-EDS) analysis. Based on these screening analyses, 10 carbonate minerals from the dolomite-ankerite series, 11 from the magnesite-siderite, and one calcite were selected as primary standards. All of these carbonates are crystalline and do not show any compositional zoning on the resolution of SEM-EDS. A subset of these reference materials was previously described as SIMS carbon and oxygen isotope standards[41,43,45]. Two grain mounts (mount 1 and mount 2), each containing multiple grains of all reference materials embedded in epoxy, were prepared and used for electron microprobe analysis and SIMS analysis.

View Article Online
DOI: 10.1039/D6JA00136J

A dolomite (H884) from a dolomite-amethyst assemblage was used to evaluate the accuracy of our matrix-effect calibrations for C, Mg, and Ca isotope measurements. Millimeter sized dolomite grains occupy the interstitial spaces of amethyst crystals in this assemblage. Several grains were carefully extracted. A subset was reserved for bulk isotopic analyses, and multiple grains were embedded in both epoxy mounts alongside primary standards. H884 dolomite exhibits pronounced Fe-Mn compositional zoning (see **Accuracy test** section), making it an appropriate analogue for zoned carbonates in carbonaceous chondrites.

Electron Microprobe

Major cation chemistry of ion microprobe carbonate standards was determined using a field-emission electron microprobe (JEOL JXA-iHP200F "Hyperprobe") in WDS mode at California Institute of Technology, following established methods[47]. Analytical conditions were 15 kV accelerating voltage, 10 nA beam current, and 10 μm defocused beam. Natural carbonate standards (calcite, dolomite, siderite, strontianite and rhodochrosite) were used to quantify Ca, Mg, Fe, Mn and Sr content in carbonates. These values are reported in **Table 1**.

True carbon isotopic composition of standards

True $\delta^{13}C$ values of all standards were measured on CO_2 liberated by overnight digestion in 103% phosphoric acid at 373 K. CO_2 was purified by passing through Nafion tubing to remove water vapor, then cryogenically trapped on a U-trap (see **Supplementary Information Section S1** for detailed digestion, purification, and gas handling protocols).

$\delta^{13}C$ values were measured using a Tunable Infrared Laser Direct Absorption Spectroscopy (TILDAS) instrument (Aerodyne Research Inc.) at Yale University. CO_2 from each standard was diluted to 408 ppm to match the laboratory reference gas and introduced into the TILDAS analyzer cell. Measurements consisted of 10 sample aliquots bracketed by reference gas aliquots (11 total), each measured for 45 seconds. International reference materials NBS-18, NBS-19, and IAEA-603 were used to provide a stretch correction, yielding uncertainties of 0.06-0.19‰ (**Table 2**). Digestion temperature (100°C) does not affect the $\delta^{13}C$ value of CO_2 during acid digestion[48]. This was confirmed by measuring Carrara Marble (PX; measured 1.94 ± 0.05‰, n=7; expected 2.01‰) and NIST SRM 88b dolomite (measured 2.17 ± 0.04‰, n=6), which agrees exactly with the value reported from UC Riverside stable isotope laboratory[49]. This provides confidence that the digestion protocol is suitable across the range of carbonate minerals analyzed in this study.

A subset of standards was independently analyzed by conventional phosphoric acid digestion (90°C, 20 min) and gas-source mass spectrometry (Thermo MAT 253 dual-inlet IRMS) at California Institute of Technology, following established protocols (see **Supplementary Information Section S2** for details). $\delta^{13}C$ values from both methods agree on a 1:1 line (**Fig. S1**), confirming the accuracy of TILDAS measurements. True $\delta^{13}C$ values reported in **Table 2** are TILDAS values unless otherwise noted.

True magnesium isotopic composition of standards

$^{26}Mg/^{24}Mg$ ratio of standards were measured by MC-ICP-MS (Thermo Neptune XT) at the University of Chicago, following established protocols. Samples were dissolved overnight in 5% HNO_3 at 65°C in a sonicated water bath, diluted in deionized water, and processed via a Thermo/Dionex ion chromatography (IC) system using 30 mM methanesulfonic acid eluent to separate Mg from matrix elements (see **Supplementary Information Section S3** for detailed column chemistry and IC separation protocols).

View Article Online
DOI: 10.1039/D6JA00136J

For samples with more than 13 mol% $FeCO_3$ ("high-Fe" samples), the IC guard column was insufficient to remove Fe, causing elution time shifts. These samples were pre-processed to remove Fe by offline anion-exchange chromatography (Bio-Rad AG1-X8 resin, 100-200 mesh) following established protocols (see **Supplementary Information Section S3**). Through this pre-processing, we completely removed Fe from all samples, with column Mg yield of 100 ± 5.5% (1SD) (see **Supplementary Information Section S3** for procedure). Due to the low Mg concentration in calcite (~0.43 mol% $MgCO_3$), Ca and Mg were first separated by offline cation-exchange chromatography using established protocols (see **Supplementary Information Section S3** for details), and subsequently processed through the IC system as described above.

For isotopic analysis, samples (~150 ppb Mg in 2% HNO_3) were introduced via a dual-path glass cyclonic spray chamber into the Neptune XT MC-ICP-MS using established protocols (see **Supplementary Information Section S3** for details). Mg solution of known isotopic composition was used as bracketing standard[50]. IHD[50], RUB[51], and seawater[50] standards were used to convert measured $^{26}Mg/^{24}Mg$ ratios to the DSM-3 scale in delta notation (per mille, ‰):

$$\delta^{26}Mg\ (‰) = [(^{26}Mg/^{24}Mg)_{sample} / (\ ^{26}Mg/^{24}Mg)_{DSM\text{-}3} - 1] \times 1000$$

True calcium isotopic composition of standards

Sample preparation for MC-ICP-MS measurements was conducted in GAIA Lab (Geoscience Applications of Isotopic Analysis), Duke University and the Duke University Shared Materials Instrumentation Facility (SMIF). Sample powders (4-25 mg) were dissolved in 0.5M HNO_3, and Ca was purified using DGA resin (Eichrom) in a prepFAST MC (ESI) automated ion-exchange chromatography system, following established protocols[52]. Purified Ca fractions were evaporated to dryness, treated twice with a 1:1 mixture of 15 M HNO_3 and 31% H_2O_2 at 120°C overnight, then dissolved in 2% HNO_3 and diluted to 2 mg/L Ca for isotopic analysis (see **Supplementary Information Section S4** for details).

Isotope ratios were measured on a Sapphire MC-ICP-MS (Nu Instruments) using established instrumental settings[53]. Ca SPEX CertiPrep (lot # CL15-24CAY) was used as a bracketing standard. All data are reported as $\delta^{44/40}Ca$ against NIST SRM 915a in delta notation (per mille, ‰):

$$\delta^{44/42}\ Ca\ (‰) = [(^{44}Ca/^{42}Ca)_{sample} / (^{44}Ca/^{42}Ca)_{standard} - 1] \times 1000$$

$$\delta^{44/40}\ Ca = \delta^{44/42}\ Ca \times 2.05 \text{ (assuming no radiogenic } ^{40}Ca \text{ excess)}$$

$\delta^{44/40}$ Ca (or, $\delta^{44}Ca$) values were converted from the IAPSO seawater scale to NIST SRM 915a following[54]:

$$\delta^{44}Ca_{seawater} + 1.88 = \delta^{44}Ca_{NIST\ SRM\ 915a}$$

SIMS analysis

Carbon isotope analysis

SIMS carbon isotope analyses of carbonates were conducted using a Cameca IMS 7f-GEO at California Institute of Technology. The primary Cs^+ ion beam (+9 kV) was set to 500 pA intensity and 10 μm in diameter on the sample surface, generating secondary ^{12}C ions (~6×10^5 cps). An electron gun was used for charge neutralization. The two carbon isotopes (^{12}C, ^{13}C) were detected using an electron multiplier (EM) detector in peak-jumping mode at mass resolving power (MRP, defined as 10% height) of 3002. A single analysis took ~11 min: 100s pre-sputtering, 20 s

View Article Online
DOI: 10.1039/D6JA00136J

secondary ion beam centering and mass calibration (including wait time), and 540 s signal acquisition (18 s × 30 cycles). Analyses were conducted over two analytical sessions using identical analytical conditions.

An Fe-free dolomite (7920) served as the running standard, with external reproducibility of ~1.2-2.2‰ (2SD) for $\delta^{13}C$. Instrumental mass fractionation (IMF) for $\delta^{13}C$ analysis is calculated as:

$$^{13}\text{IMF (‰)} = \left[\frac{\left({}^{13}C/{}^{12}C \right)_{\text{SIMS}}}{\left({}^{13}C/{}^{12}C \right)_{\text{True}}} - 1 \right] \times 1000$$

where the subscripts "True" and "SIMS" indicate isotopic ratios from bulk chemical analysis and that measured by SIMS, respectively (hereon).

Magnesium isotope analysis

SIMS magnesium isotope analyses of carbonates were conducted using a Cameca IMS 7f-GEO at California Institute of Technology, over two sessions with different analytical conditions. In the first session, the primary O^- ion beam was accelerated by 22 kV (−13.5 kV at the ion source and +8.5 kV at the sample surface) and was focused to ~20 μm in diameter at 15 nA for pre-sputtering, generating secondary ^{24}Mg ions (~2×10^7 cps for dolomite, ~1×10^8 cps for magnesite), followed by analysis with a 10 nA beam. Two stable isotopes of magnesium (^{24}Mg, ^{26}Mg) were detected using a faraday cup (FC) in peak-jumping mode at MRP of 2000 (entrance slit; 218 μm and energy slit 47 μm). A single analysis took ~10 min: 120s pre-sputtering, 208 s secondary ion beam centering, and mass calibration (including wait time), and 292 s signal acquisition (5.8 s × 50 cycles).

In the second session, a lower beam current was used with slightly differing conditions for dolomite-ankerite and magnesite-siderite series minerals. The primary O^- ion beam was focused to ~15 μm in diameter at 3 nA for pre-sputtering, generating secondary ^{24}Mg ions (~3×10^6 cps for dolomite, ~5×10^6 cps for magnesite), followed by analysis with a 3 nA (dolomite) or 1 nA (magnesite) beam. Three stable isotopes of magnesium were detected: ^{24}Mg using a Faraday cup (FC), and ^{25}Mg and ^{26}Mg using an electron multiplier (EM) detector in peak-jumping mode at MRP of 3519 (entrance slit 109 μm, energy slit 47 μm), to ensure resolution of the ^{25}Mg peak from $^{24}Mg^1H$ interference. A single analysis took ~12 min: 120 s pre-sputtering, 208 s secondary ion beam centering and mass calibration (including wait time), and 392 s signal acquisition (9.8 s × 40 cycles). EM dead time correction was applied to $^{25,26}Mg$.

An Fe-free dolomite (7920) served as the running standard for dolomite-ankerite minerals while Fe-free magnesite (MRR 1077) served as the running standard for magnesite-siderite minerals. External reproducibility for $\delta^{26}Mg$ of 7920 dolomite and MRR 1077 magnesite were ~0.6‰ (2SD) and ~0.4‰ (2SD), respectively. Instrumental mass fractionation (IMF) for $\delta^{25,26}Mg$ analysis is calculated as:

$$^{i}\text{IMF (‰)} = \left[\frac{\left({}^{i}Mg/{}^{24}Mg \right)_{\text{SIMS}}}{\left({}^{i}Mg/{}^{24}Mg \right)_{\text{True}}} - 1 \right] \times 1000 \; ; \; i=25, 26$$

We also evaluated ^{26}IMF for a calcite standard in the first session. Due to its low Mg content (~0.43 mol% $MgCO_3$), the Mg yield was too low to be detected by a FC. Therefore, ^{24}Mg

View Article Online
DOI: 10.1039/D6JA00136J

and ^{26}Mg were detected using an electron multiplier (EM) with longer counting times. The primary O^- ion beam was focused to ~20 μm in diameter at 10 nA for pre-sputtering, generating secondary ^{24}Mg ions (~1 × 10^5 cps), followed by analysis at 10 nA. Two stable isotopes of magnesium (^{24}Mg, ^{26}Mg) were detected using an EM in peak-jumping mode at MRP of 2000 (entrance slit 218 μm; energy slit 47 μm). A single analysis took ~40 min: 120 s pre-sputtering, 208 s secondary ion beam centering and mass calibration (including wait time), and 2016 s signal acquisition (6.7 s × 300 cycles). Mass calibration was repeated every 100 cycles. Dolomite or magnesite bracketing standards were not measured as their ^{24}Mg yield (2 × 10^7 - 1×10^8 cps/nA) is too high for reliable EM detection and risks saturating or degrading the EM detector. For this reason, we present absolute ^{26}IMF for the calcite standard rather than expressing it relative to dolomite or magnesite.

Calcium isotope analysis

SIMS calcium isotope analyses of dolomite-ankerite minerals and calcite were conducted using a Cameca IMS 7f-GEO at California Institute of Technology. The primary O^- ion beam was accelerated by 22 kV (−13.5 kV at the ion source and +8.5 kV at the sample surface) and was focused to ~10 μm in diameter at 3 nA for pre-sputtering, generating secondary ^{40}Ca ions (~4 × 10^6 cps), followed by analysis with a 2.5 nA beam. The two stable isotopes of calcium (^{44}Ca and ^{40}Ca) were detected using a Faraday cup (FC) and an electron multiplier (EM) detector, respectively, at MRP of 3996 (entrance slit; 65 μm and energy slit 47 μm).

A series of isobaric interferences on the $^{40}Ca^+$ or $^{44}Ca^+$ peak can impact Ca isotope analysis of carbonates[46] (see their **Table 2**). At the MRP used in this study, all interferences were resolved except three:

(1) *Contribution of $^{88}Sr^{2+}$ to the $^{44}Ca^+$ peak* (requires MRP ~18,000): Because our carbonate standards are nearly Sr-free (**Table 1**), this interference contributes negligibly to our measurements. For Sr-free calcite, this contribution is <0.04 ‰, based on a previous study[46]. Therefore, we did not attempt to resolve this interference.

(2) *Contribution of $^{40}K^+$ to the $^{40}Ca^+$ peak* (requires MRP ~28,000): Our standards have no measurable potassium based on WDS analysis, and show negligible $^{39}K^+$ counts in SIMS. The contribution of $^{40}K^+$ to the $^{40}Ca^+$ peak of carbonates has been found to be negligible in previous work[46], and we did not attempt to resolve this interference.

(3) *Contribution of $^{39}K^1H^+$ peak to $^{40}Ca^+$* (requires MRP ~4,470): Given the nearly K-free nature of our standards and previous findings on calcite[46], this contribution is also estimated to be negligible. Resolving this interference would have significantly increased the analytical time per spot and was therefore not attempted.

A single analysis took ~16 min: 120s pre-sputtering, 216 s secondary ion beam centering and mass calibration (including wait time), and 624 s signal acquisition (10.4 s × 60 cycles). EM dead time correction was applied.

An Fe-free dolomite (7920) served as the running standard, with external reproducibility for δ^{44}Ca of ~0.8‰ (2SD). Instrumental mass fractionation (IMF) for δ^{44}Ca analysis is calculated as:

$$^{44}\text{IMF (‰)} = \left[\frac{\left(^{44}\text{Ca}/_{^{40}\text{Ca}}\right)_{\text{SIMS}}}{\left(^{44}\text{Ca}/_{^{40}\text{Ca}}\right)_{\text{True}}} - 1\right] \times 1000$$

Data processing and working calibration construction

View Article Online
DOI: 10.1039/D6JA00136J

Measured δ_{raw} values (raw isotope ratios measured by SIMS, expressed in per mille) were processed following previously described protocols[43]. Briefly, for every isotopic system, δ_{raw} values are corrected for background, instrumental drift and detector dead time where applicable. Instrumental drift was monitored and corrected using multiple drift-correction standards analyzed throughout all analytical sessions. The corrected values (hereon, δ_{SIMS}) are then converted to IMF following the equations in the previous sections. Absolute IMF values for a reference material can vary between sessions, as they are sensitive to specific analytical conditions (i.e., instrumental tuning conditions). To facilitate comparison of IMF across sessions, a normalization scheme is necessary. The IMF values are therefore normalized relative to the drift monitor material for each session (commonly, pure dolomite and magnesite for dolomite-ankerite and magnesite-siderite minerals, respectively). This relative IMF (hereon, IMF*, **Tables 3-5**) is defined as:

$$\text{IMF*}\ (‰) = \left[\frac{(1+\text{IMF}_{\text{RM}}/1000)}{(1+\text{IMF}_{\text{DMM}}/1000)} - 1\right] \times 1000$$

where subscripts RM and DMM denote reference material and drift monitor material, respectively. We therefore focus our discussions on the variability of IMF* rather than absolute IMF values. Analytical uncertainty on IMF*, including spot-to-spot reproducibility of the standard and the analytical uncertainty of the bracketing drift-monitor standards propagated in quadrature, is presented in **Tables 3-5**. The isotopic heterogeneity of each grain is estimated using the 1SD of the IMF* values for each reference material.

The SIMS matrix effect for solid solution minerals is constructed by comparing the IMF* against different compositional parameters. For minerals with high-dimensional compositional spaces, such as garnet, IMF must be evaluated against multiple end-member mol fractions simultaneously[55–58]. The case for carbonates is simpler. Due to multiple solvi in the Ca-Mg-Fe carbonate ternary system[59,60], most natural compositions are limited to Ca-carbonates (e.g., calcite, aragonite), dolomite-ankerite or magnesite-siderite series, where mol fraction of $CaCO_3$ is fixed. In each carbonate series considered in this study, mol fraction of $CaCO_3$ is fixed by crystal chemistry (~0.5 for dolomite-ankerite; ~0 for magnesite-siderite, **Table 1**). With mol fraction of $CaCO_3$ fixed, the molar contributions of remaining cations (Mg, Fe, Mn) must sum to a constant, reducing the compositional space to exactly two independent degrees of freedom: mol fraction of $FeCO_3$ and $MnCO_3$ (whose sum is complementary to $MgCO_3$ mol fraction, since all three must sum to a constant). In our primary standards, mol fractions of $FeCO_3$ and $MnCO_3$ are correlated (**Table 1**), meaning that their individual contributions to IMF cannot be separated from our standards alone. Therefore, we sum Fe+Mn content of carbonates ((Fe+Mn)# = molar [Fe+Mn]/molar [Fe+Mn+Mg]), which is both necessary and sufficient as the sole compositional calibration parameter for IMF. Given Fe and Mn are expected to have comparable contributions to the IMF[30,61] (possibly due to their similar atomic mass and ionic radii), this treatment is justified, and consistent with previous protocols[61].

A subset of earlier studies attributed variation of carbon and oxygen isotope IMF* of carbonates to their Fe content (Fe# = molar Fe/molar [Fe+Mg])[43–45] alone, ignoring the effect of Mn since the standards used in those studies were relatively Mn-poor. The motivation behind our study is to develop calibrations applicable to carbonates from carbonaceous chondrites, which can be substantially Mn-rich[38,40,62,63]. For this reason, we developed reference materials with greater Mn contents than previously established standards[43,45], to better match target analytes. Hence, the IMF* of our reference materials reflects contributions from both their Fe and Mn contents, and we discuss IMF* variation with (Fe+Mn)#, an appropriate approach for Mn-rich extraterrestrial carbonate analysis. It is important to note that IMF values for C and Mg isotope measurements are

View Article Online
DOI: 10.1039/D6JA00136J

negative; higher (i.e. less negative) IMF* corresponds to a lower degree of instrumental fractionation and vice versa. For Ca isotope measurements, IMF values are positive, so higher ^{44}IMF* (i.e. more positive) corresponds to a higher degree of instrumental fractionation.

We do not attempt to evaluate the effect of mol fraction of $CaCO_3$ on IMF* because appropriate standards along the calcite-dolomite-magnesite join (with fixed (Fe+Mn)#) are unavailable to us due to their rarity in nature, making an interpolation across this large compositional range highly uncertain and impossible to validate for accuracy. Additionally, since calcite, dolomite-ankerite, and magnesite-siderite are frequently analyzed under different analytical conditions in this study (e.g., for Mg isotopes), interpolation between standards measured under different conditions would be inappropriate. Constraining the effect of $CaCO_3$ mol fraction on IMF* therefore remains a tractable target for future studies, ideally using a dedicated set of synthetic or natural standards with fixed (Fe+Mn)# spanning the full molar Ca content range.

The final step of calibration construction involves empirically fitting the IMF*-(Fe+Mn)# relationship. The choice of fitting function depends on the shape of this relationship. Previous studies on C-O isotope IMF of dolomite-ankerite and magnesite-siderite minerals observed asymptotic (saturation) behavior of IMF* with increasing (Fe+Mn)#, adequately described by Hill[43,64] or logistic equations[34]. Studies on silicate minerals used sigmoidal, parabolic[31] (for ^{18}IMF* of olivines) and quadratic functions[32] (^{25,26}IMF* of olivines and pyroxenes) to describe IMF-composition relationships. Although the Hill equation remains a popular choice for describing asymptotic IMF* variations, it cannot fit parabolic relationships. Given that we observe a variety of IMF*-(Fe+Mn)# trends for different isotope systems, including parabolic ones, we use polynomial fits to describe our IMF*-(Fe+Mn)# relationships, unless otherwise specified.

Application of the working calibrations to unknown carbonates proceeds as follows. First, the major cation chemistry of each SIMS analytical spot (or an adjacent spot) is determined by EPMA, and the spot-specific (Fe+Mn)# is calculated. The drift-corrected SIMS measurement is then expressed as a ratio relative to the bracketing standard, and the corresponding IMF* is obtained from the working calibration using the measured (Fe+Mn)#. The true isotopic composition of the unknown is solved algebraically from the IMF* equation (see **Accuracy test section** for the full derivation). Propagated uncertainties include contributions from the internal measurement precision, bracketing standard reproducibility, and calibration residuals, combined in quadrature. This workflow requires that EPMA and SIMS analyses be performed on the same grain, ideally at co-located positions, to ensure that the (Fe+Mn)# used for calibration is representative of the sputtered volume.

Finally, a note on reporting conventions: throughout this study, analytical uncertainties for δ^{13}C are reported as 2SD (two standard deviations), following common practice in stable carbon isotope geochemistry, while uncertainties for δ^{26}Mg and δ^{44}Ca are reported as 1SD. This convention reflects the different community standards for these isotope systems and facilitates comparison with published data[46,63,65]. Unless otherwise stated, quoted uncertainties include contributions from internal measurement precision, reproducibility of bracketing standards, and calibration residuals, propagated in quadrature.

Results and discussion

A total of 22 standards were used to evaluate SIMS matrix effects, including one calcite, 10 dolomite-ankerite and 11 magnesite-siderite minerals. Dolomite-ankerite and magnesite-siderite minerals had (Fe+Mn)# in the range 0.002-0.731 and 0.005-0.997, respectively (**Table 1**). These standards had true δ^{13}C values from −9.7‰ to 2.8‰, δ^{26}Mg values from −5.12‰ to 0.54‰, and

View Article Online
DOI: 10.1039/D6JA00136J

δ^{44}Ca values from 0 to 1.6‰ (**Table 2**). IMF* variation of standards for all the isotope systems was studied from mount 2, except for Mg isotopes where IMF* variation was studied from both mounts.

Variation of secondary ion yield with Fe+Mn content of carbonates

Secondary ion yields vary systematically with (Fe+Mn)# of carbonate standards for all isotope systems investigated. These relationships are constrained by plotting (Fe+Mn)# of standards against the yield of the abundant stable isotope for each system (e.g., ^{12}C, ^{24}Mg, ^{40}Ca).

For carbon isotope analysis of dolomite-ankerite minerals **(Table 3)**, ^{12}C yield increased steadily from 5.2-5.9×10^5 cps/nA to 7.3-8.3×10^5 cps/nA as (Fe+Mn)# increased from 0 to 0.73 over two sessions (**Fig. 2a**). For magnesite-siderite minerals, ^{12}C yield first increased from 3.4-3.6 × 10^5 cps/nA to 5.4 × 10^5 cps/nA as (Fe+Mn)# increased from 0 to 0.5, then decreased to 2.4 × 10^5 cps/nA as (Fe+Mn)# increased from 0.5 to 1, defining a parabolic relationship (**Fig. 2b**) consistent with previous observations[45].

For magnesium isotope analysis of dolomite-ankerite minerals **(Table 4)**, ^{24}Mg yield showed a parabolic relationship with (Fe+Mn)#, peaking near (Fe+Mn)# ~ 0.2 (**Fig. 2c**). This pattern was reproduced across two mounts in the first session (10 nA) and at lower absolute yield in the second session (1 nA). For magnesite-siderite minerals **(Table 4)**, ^{24}Mg yield remained relatively invariant from (Fe+Mn)# = 0 to 0.12, then gradually decreased at higher (Fe+Mn)# in session 1 (10 nA). In session 2 (1nA), a parabolic relationship was observed with a maximum near (Fe+Mn)# ~0.13 (**Fig. 2d**).

For calcium isotope analysis of dolomite-ankerite minerals **(Table 5)**, ^{40}Ca yield increased from 4.2 × 10^6 cps/nA to 6.8 × 10^6 cps/nA as (Fe+Mn)# increased from 0 to 0.64, then decreased slightly to 6.3 × 10^6 cps/nA as (Fe+Mn)# = 0.73, defining a parabolic relationship (**Fig. 2e**).

The observed trends are governed by two competing processes: (1) a "conductivity effect", whereby increasing Fe content enhances the electrical conductivity of carbonates, leading to more efficient sputtering and higher secondary ion yields; and (2) a "concentration effect", whereby the concentration of an element (e.g., Mg) decreases with increasing Fe substitution due to stoichiometric constraints, reducing the secondary ion yield. Where yield-(Fe+Mn)# relationships define a parabolic trend, the conductivity effect initially dominates until a maximum yield is reached, beyond which the concentration effect takes over.

Variation of IMF with Fe+Mn content of carbonates

For all isotope systems investigated, IMF* values show strong, non-linear correlations with (Fe+Mn)# of standards. These relationships were empirically modelled using polynomial or sigmoidal functions, yielding regression R^2 values of 0.92-0.99 and calibration residuals with zero mean and 1SD of 0.1-0.7‰ (**Table 6**). In all cases, calibration residuals were uncorrelated with (Fe+Mn)#, confirming that secondary matrix-effect corrections are not required. Below, we describe the key features of each isotope system. Complete data are provided in **Tables 3-6** and **Figs. 3-7**.

C isotopes

Dolomite-ankerite series

^{13}IMF* (relative to 7920 dolomite) for the dolomite-ankerite minerals spans a 5‰ range **(Table 3)**. ^{13}IMF* shows a non-linear variation with (Fe+Mn)#: an initial decrease from 0‰ to −5‰ as (Fe+Mn)# increases from 0 to 0.19, followed by a recovery to −1‰ at (Fe+Mn)# = 0.52 and

View Article Online
DOI: 10.1039/D6JA00136J

relative invariance to 0.73. This trend is reproduced between two analytical sessions with identical conditions (**Fig. 3a**).

The general direction and range of the ^{13}IMF*-(Fe+Mn)# variation is consistent with previous findings[44]. However, those studies, performed on a large-radius SIMS, reported an asymptotic decrease of ^{13}IMF* with increasing (Fe+Mn)#[44], which is different from the parabolic relationship observed here (**Fig. 3a**). The parabolic shape is largely driven by the low ^{13}IMF* of 15086 dolomite ((Fe+Mn)# = 0.19). To verify that this is not an artifact, we confirmed that: (a) 15086 was analyzed 12 times across two sessions from different regions of a millimeter-sized grain, all yielding consistently low ^{13}IMF*, ruling out isotopic heterogeneity or instrumental variability; (b) its true $\delta^{13}C$ was measured independently by both TILDAS and gas-source IRMS with consistent results (**Table 2**, **Fig. S1**); and (c) its major-cation composition is homogeneous based on multiple EPMA analyses (**Table 1**). We therefore consider the parabolic ^{13}IMF*-(Fe+Mn)# relationship to be a genuine feature of this analytical setup. We attribute the discrepancy with previous work to the different instrumental configurations involved: the small-radius IMS 7f-GEO used in this study differs from the large-radius IMS-1280 used previously in instrument geometry and secondary ion optics, primary Cs^+ beam acceleration voltage (9 kV vs. 10 kV), beam size (10 μm vs. 6 μm), transmission characteristics, and energy bandpass – all of which affect the secondary ion population reaching the detector and the sputtering/ionization physics underpinning IMF. Additionally, the detection scheme in the previous study[44] employed a Faraday cup for ^{12}C but an axial electron multiplier for ^{13}C, meaning EM dead time considerations apply to that dataset as well, albeit asymmetrically. Analogous instrument-dependent IMF trends have been documented for O isotopes in olivines[31], garnet[55,56,58,66] and for ^{25,26}Mg in olivines and pyroxenes[32], where parabolic and quadratic IMF*-composition trends have been observed using FC-FC detection. Therefore, different SIMS instruments (e.g., IMS 7f GEO vs. IMS 1280) and detection schemes (e.g., FC-FC, FC-EM, EM-EM) can yield distinct functional forms of IMF*-composition relationships, not merely different magnitudes, highlighting that IMF* calibrations are instrument-specific, and should not be transferred between different SIMS instruments without independent verification.

3rd-order polynomials fitted to the ^{13}IMF*-(Fe+Mn)# data yield R^2 values of 0.92 (session 1) and 0.95 (session 2) (**Fig. 3a, Table 6**). Calibration residuals average of 0.0±0.46‰ (1SD, session 1) and 0.0±0.38‰ (1SD, session 2) (**Table 6**), and are uncorrelated with (Fe+Mn)# of reference materials (**Fig. 3b,c,**). These residuals are larger than those achieved on a large-radius SIMS (≤0.3‰)[43]. A plausible explanation is the superior secondary ion signal stability of large-radius instruments, where magnetic field drift is mitigated by additional magnetic field measurement devices (e.g., Hall probe or NMR probe) and associated feedback mechanisms. The IMS 7f-GEO used in this study lacks such a device, which likely contributes to larger secondary ion signal variability and overall higher calibration residuals. This consideration applies to all isotope systems investigated in this study.

Magnesite-siderite series

^{13}IMF* for the magnesite-siderite minerals spans a 7‰ range **(Table 3)**. ^{13}IMF* decreases gradually from –2‰ to –9‰ as (Fe+Mn)# increases from 0 to 0.3, and remains relatively invariant thereafter to (Fe+Mn)# ~1. This trend is reproduced between two sessions with identical analytical conditions, with the ^{13}IMF*-(Fe+Mn)# relationships from both sessions overlapping within analytical uncertainty (**Fig. 3d**). The general direction and curvature of the ^{13}IMF*-(Fe+Mn)# variation is consistent with previous findings[45]. However, those previous studies, performed on a

View Article Online
DOI: 10.1039/D6JA00136J

large radius SIMS, reported an 11‰ range in ^{13}IMF*, compared to 7‰ here (**Fig. 3d**). As discussed above, this difference likely stems from different instrumental conditions.

3rd-order polynomials yield R^2 values of 0.93 (session 1) and 0.95 (session 2) (**Fig. 3d, Table 6**). Calibration residuals average of 0.0 ± 0.64‰ (1SD, session 1) and 0.0 ± 0.50‰ (1SD, session 2), and are uncorrelated with (Fe+Mn)# (**Fig. 3e,f**). These are the largest calibration residuals among all systems studied here (ranging 1.6‰ in both sessions). On a large-radius SIMS, residuals for magnesite-siderite ^{13}IMF are slightly better (≤0.5‰)[45].

The total propagated uncertainty for a single $\delta^{13}C$ analysis, combining calibration residuals, internal measurement precision, and bracketing standard reproducibility, is approximately 2.0-2.3‰ (2SD). This limits the application of our C isotope protocol to geological settings where $\delta^{13}C$ varies by several per mille; a condition met by most low-temperature carbonate systems of interest, including the extraterrestrial targets that motivate this study.

Mg isotopes

Dolomite-ankerite series

^{26}IMF* for the dolomite-ankerite minerals cover a 20-24‰ range **(Table 4)**, the largest matrix effect observed in this study. In session 1 (10 nA beam current), ^{26}IMF* (relative to 12700 dolomite since 7920 dolomite was not mounted in this block) in mount 1 increased rapidly to 22.1‰ as (Fe+Mn)# from 0 to 0.52, then shows a more limited increase to 24‰ as (Fe+Mn)# reaches 0.73 (**Fig. 4a**). ^{26}IMF* (relative to 7920 dolomite) in mount 2 showed a similar behavior (**Fig. 4b**) although with smaller magnitude. In session 2 (3 nA beam current), ^{26}IMF* (relative to 7920 dolomite) increased from 0‰ to 22.1‰ and ^{25}IMF* (relative to 7920 dolomite) increases from 0‰ to 12‰ steadily with increasing (Fe+Mn)# from 0-0.73 (**Fig. 4c,d**). Variations in ^{26}IMF* and ^{25}IMF* follow a terrestrial fractionation law, where the variation of ^{25}IMF* is approximately half that of corresponding ^{26}IMF* for a given reference material (**Fig. 4e**).

3rd-order polynomials adequately describe the ^{26}IMF*-(Fe+Mn)# relationship in both sessions. For session 1, R^2 values are 0.998 (mount 1) and 0.999 (mount 2) (**Fig. 4a,b**), with calibration residuals averaging 0.0 ± 0.42‰ (1SD, mount 1) and 0.0 ± 0.12‰ (1SD, mount 2) (**Table 6**). Residuals are uncorrelated with (Fe+Mn)# (**Fig. 4a,b,** bottom panels). For session 2, R^2 values are 0.998 (^{26}IMF*) and 0.996 (^{25}IMF*) (**Fig. 4c,d**), with calibration residuals averaging 0.0 ± 0.20‰ (1SD) for both ^{25,26}IMF* (**Table 6**). Residuals are again uncorrelated with (Fe+Mn)# (**Fig. 4c,d**, bottom panels). For comparison, a large-radius SIMS can achieve Mg isotope calibration precision of 0.1‰ (1SD) or better for silicate minerals[32], which is better than what we achieved in this study.

Magnesite-siderite series

^{26}IMF* for the magnesite-siderite minerals spans a 19.1-19.6‰ range **(Table 4)**. In session 1 (10 nA beam current), ^{26}IMF* (relative to 2123 magnesite) increases sharply to 10.7-11.3‰ as (Fe+Mn)# increases from 0 to 0.12, then increases more slowly to 19.1-19.6‰ as (Fe+Mn)# reaches 0.8 (**Fig. 5a,b**), consistently across two mounts. In session 2 (1 nA beam current), ^{26}IMF* (relative to MRR1077 magnesite) increases more gradually from 0‰ to 18.7‰ and ^{25}IMF* (relative to MRR1077 magnesite) from 0‰ to 7.9‰ with increasing (Fe+Mn)# from 0 to 0.5, remaining relatively invariant as (Fe+Mn)# increased to 0.8 (**Fig. 5c,d**). Variations in ^{26}IMF* and ^{25}IMF* follow a terrestrial fractionation law (**Fig. 5e**).

For session 1, a 3rd- or 4th-order polynomial fit to the ^{26}IMF*-(Fe+Mn)# data resulted in overfitting between (Fe+Mn)# = 0.12-0.5, a region lacking analytical data because standard SMS9

View Article Online
DOI: 10.1039/D6JA00136J

((Fe+Mn)# = 0.321) was not analyzed in this session. This also resulted in poor fit (R^2 <0.98) and larger residuals (up to 1‰). To avoid this, we described the ^{26}IMF*-(Fe+Mn)# relationship from both mounts using a symmetric sigmoidal function (similar to the Hill equation used in previous studies[43–45]) having functional form:

$$^{26}\mathrm{IMF}^{*} = d + \frac{a - d}{1 + \left(\frac{[\mathrm{Fe} + \mathrm{Mn}]\#}{c}\right)^{b}}$$

where coefficients *a*, *b*, *c*, *d* are evaluated iteratively, following previously described procedures[43]. This yielded improved R^2 values of 0.998 (mount 1) and 0.999 (mount 2) (**Fig. 5a,b**), with calibration residuals averaging 0.0 ± 0.35‰ (1SD, mount 1) and 0.0 ± 0.19‰ (1SD, mount 2) (**Table 6**). Residuals are uncorrelated with (Fe+Mn)# (**Fig. 5a,b,** bottom panels).

In session 2, ^{25,26}IMF*-(Fe+Mn)# data from the second mount could be adequately described by 3rd-order polynomials, yielding R^2 = 0.999 for both ^{25}IMF* and ^{26}IMF* (**Fig. 5c,d**), with calibration residuals averaging 0.0 ± 0.14‰ (1SD, ^{26}IMF*) and 0.0 ± 0.13‰ (1SD, ^{25}IMF*) (**Table 6**). Residuals are uncorrelated with (Fe+Mn)# (**Fig. 5c,d,** bottom panels).

Calcite

We analyzed 22 points on the calcite grain. Over these 22 analyses, the ^{26}IMF varied from –48.3‰ to –49.9‰, covering a 1.6‰ range (**Fig. 6**). The average ^{26}IMF value of all the analyses was –49.1 ± 0.46‰ (1SD, n=22). This value is absolute (not normalized to a dolomite or magnesite bracket) and was measured under different detector conditions (EM for both isotopes), as described in the **Methods** section. It therefore cannot be directly compared to the dolomite-ankerite or magnesite-siderite calibrations, and calcite requires separate end-member standardization for Mg isotopes.

Ca isotopes

Dolomite-ankerite series

Ca isotope analysis was performed on dolomite-ankerite minerals and calcite only, given the negligible Ca content of magnesite-siderite minerals (<1-2 mol% $CaCO_3$, **Table 1**). ^{44}IMF* (relative to 7920 dolomite) for the dolomite-ankerite minerals spans a 6‰ range (**Table 5**). ^{44}IMF* remains invariant around 0.5‰ as (Fe+Mn)# increases from 0 to 0.53, then rises rapidly to 5.9‰ as (Fe+Mn)# reaches 0.74, defining an exponential-like increase (**Fig. 7**). A 4th-order polynomial fitted to the ^{44}IMF*-(Fe+Mn)# data yields R^2 = 0.99 (**Fig. 7, Table 6**), with calibration residuals averaging 0.0 ± 0.23‰ (1SD) (**Table 6**). Residuals are uncorrelated with (Fe+Mn)# (**Fig. 7,** bottom panel). We note that this calibration is based on a single analytical session. Reproducing it in additional sessions would strengthen confidence in its robustness.

Calcite

^{44}IMF* (relative to 7920 dolomite) for the calcite standard was –19.0 ± 0.5‰ (1SD, n = 3) and –18.7 ± 0.6‰ (1SD, n = 8) for two brackets within the same analytical session, with an average ^{44}IMF* of –18.8 ± 0.4‰ (1SD, n = 11) (**Table 5**).

Accuracy test

Overall approach

View Article Online
DOI: 10.1039/D6JA00136J

Due to the large IMF* variations and their high sensitivity to the (Fe+Mn)# of standards, it is critical to evaluate whether our working calibrations can yield accurate analyses of natural unknowns. Previous studies demonstrated accuracy using compositionally homogeneous natural carbonates, usually end member Ca-Mg-Fe carbonates[46,34]. However, homogeneous end-member materials do not represent the complexity of natural samples with micron-scale compositional zoning, which the protocol aims to analyze. Additionally, accuracy demonstrated on end-member carbonates does not guarantee the accuracy of the IMF*-(Fe+Mn)# calibrations across the solid solution, which requires either zoned secondary standards or multiple natural carbonates spanning a wide range in (Fe+Mn)#, with true isotopic compositions independently characterized at least at grain-scale.

This distinction is particularly important because the calibrations are empirical fits interpolating between standards. If there are fine-scale variations of IMF* between standards that are underestimated by the fits – especially in the compositional range where analytes of interest lie – this can result in inaccurate SIMS measurements. One approach would be to sample the IMF*-(Fe+Mn)# relationship at higher resolution by adding intermediate dolomite-ankerite and magnesite-siderite standards. However, the rarity of such minerals with homogeneous, well-characterized isotopic compositions makes this impractical. It is therefore essential to test the accuracy of the working calibrations in the compositional range where target analytes lie and/or where IMF* evolves most strongly with (Fe+Mn)#, which has not been done in previous studies.

A dolomite (H884) was used to test the C, Mg, and Ca isotope calibrations. This dolomite exhibits pronounced compositional zoning: across ~1.5 mm length of a single grain, the $FeCO_3$ content (mol fraction) varies from 0.04 to 0.12 with co-varying $MnCO_3$ content (mol fraction) from 0.01-0.03 (**Fig. 8a,b**). This grain is compositionally similar to dolomites from CM-CI chondrites[40,63,67] and Martian meteorites[68] (**Fig 1, 8c**), and lies in the compositional region where IMF*-(Fe+Mn)# variation is largest for C and Mg isotopes (**Fig. 3,4**). These properties make it an ideal representative for zoned carbonates from carbonaceous chondrites, and an excellent material for evaluating the accuracy of our C, Mg, and Ca isotope calibrations.

Terrestrial breunnerites that match the composition of those from CI chondrites are rare, and not available to us. Therefore, we used a Mg-siderite 10937 to test our magnesite-siderite C isotope calibration. This material is compositionally homogeneous (**Table 1**) with $FeCO_3$ content (mol fraction) 0.86 and $MnCO_3$ content (mol fraction) of 0.04 and (Fe+Mn)# = 0.89. To test the accuracy of our magnesite-siderite Mg isotope calibration, we use compositionally homogeneous end-member magnesite (treating MRR1077 as unknown in one session) and intermediate magnesite (RK-1 magnesite, (Fe+Mn)# = 0.06; **Table 1**).

Application of the IMF*-(Fe+Mn)# calibrations to unknown carbonates requires knowledge of the major cation chemistry at or near each SIMS analytical spot. For the accuracy test on zoned dolomite H884, electron microprobe analyses were performed along transects across the same grain prior to SIMS analysis, using a 10 μm defocused beam. SIMS pits were subsequently placed adjacent to the nearest EPMA spots. For compositionally homogeneous materials, multiple EPMA analyses were conducted across multiple grains to determine grain-average composition (**Table 1**).

We analyzed C, Mg and Ca isotopic compositions of multiple spots along transects across the Fe-Mn zoning on a zoned H884 grain (**Fig. 8a**), along with 10937 and RK-1 magnesite using SIMS. For each isotope system, the raw SIMS data (δ_{raw}, ‰) were first drift-corrected and expressed relative to the bracketing standard (7920 dolomite for C, Ca; 12700 dolomite for Mg) as a ratio:

View Article Online
DOI: 10.1039/D6JA00136J

$$^{x}R_{SIMS\ (SMP/STD)} = \frac{\left(1+\frac{\delta^{x}_{raw}}{1000}\right)_{SMP}}{\left(1+\frac{\delta^{x}_{raw}}{1000}\right)_{STD}}$$

where x = 13, 26, 44 for C, Mg, Ca isotope systems, respectively. Similarly, the ratio of their true isotopic compositions (δ_{true} relative to VPDB, DSM-3, and SRM-915a for C, Mg, and Ca isotopes respectively, in ‰, **Table 2**) is expressed as:

$$^{x}R_{TRUE\ (SMP/STD)} = \frac{\left(1+\frac{\delta^{x}_{true}}{1000}\right)_{SMP}}{\left(1+\frac{\delta^{x}_{true}}{1000}\right)_{STD}}$$

The ratio of these two ratios is related to the ^{x}IMF* as:

$$\left(1+\frac{^{x}IMF^{*}}{1000}\right) = \frac{^{x}R_{SIMS\ (SMP/STD)}}{^{x}R_{TRUE\ (SMP/STD)}} = \frac{\frac{\left(1+\frac{\delta^{x}_{raw}}{1000}\right)_{SMP}}{\left(1+\frac{\delta^{x}_{raw}}{1000}\right)_{STD}}}{\frac{\left(1+\frac{\delta^{x}_{true}}{1000}\right)_{SMP}}{\left(1+\frac{\delta^{x}_{true}}{1000}\right)_{STD}}}$$

where ^{x}IMF* are calculated from the working calibrations using spot-specific (Fe+Mn)#. Since all other variables are known, δ_{true} value for sample – the only unknown – was calculated from this equation. Reported propagated uncertainties for each point (**Tables 7, 8**) include contributions from the internal error of each analysis, the bracketing standard reproducibility, and the residuals of the working calibration, propagated in quadrature.

Statistical approach for evaluating grain-average accuracy

The purpose of this accuracy test is to evaluate whether the mean of multiple corrected SIMS analyses agrees with the independently measured bulk value. The appropriate metric for this comparison is the standard error (SE) of the mean, rather than the standard deviation of individual analyses. For zoned dolomite H884, the SD of corrected SIMS analyses reflects both real isotopic variation across the zoning and analytical uncertainty; it does not describe how well the mean is constrained. We therefore report grain-average SIMS values with 2SE uncertainties, enabling a rigorous comparison with the bulk measurement.

An important caveat applies to this comparison: the SIMS grain average is an unweighted spatial average along a linear transect, whereas the bulk measurement is a volume-weighted average of the entire grain. If the transect over- or under-samples certain compositional zones relative to their volumetric proportion, the two means may not be strictly equivalent even with perfect analytical accuracy. This sampling bias is an inherent limitation of comparing transect-based SIMS averages to bulk values.

C isotopes

View Article Online
DOI: 10.1039/D6JA00136J

H884 Dolomite

We analyzed $\delta^{13}C$ of 29 points across the Fe-Mn zonation along a transect from Fe-poor to Fe-rich zones of a single H884 grain from mount 2, achieving internal error of ~1.7‰ (2SD) per analysis. Across the (Fe+Mn)# range of 0.12-0.33, corrected $\delta^{13}C$ values varied from 1.9 ± 2.2‰ (2SD) to −12.8 ± 2.3‰ (2SD) (**Fig. 9a, Table 7**), reflecting the isotopic or thermal evolution of the parent fluid. The SD of all corrected $\delta^{13}C$ values is 3.2‰, which includes both geological variability across the zoning profile and analytical scatter.

The grain-average $\delta^{13}C$ value measured by SIMS was −6.2 ± 1.2‰ (2SE, n = 29), compared to the true grain-average $\delta^{13}C$ measured by phosphoric acid digestion of −8.3 ± 0.4‰ (2SE, n = 2) (**Fig. 9a, Table 7**). The offset between the two means is 2.1‰, which exceeds the 2SE of the SIMS mean alone but considering the combined uncertainty of the two measurements propagated in quadrature (2SE=1.3‰, $\delta^{13}C$ offset/combined 2SE ~1.7), we see agreement at the ~2SD level. Part of this offset may reflect the sampling bias inherent in comparing a linear transect average to a volume-weighted bulk value. If the transect moderately over-samples Fe-rich zones (which tend to have lower $\delta^{13}C$), even a ~10-15% volumetric over-representation of such zones could shift the transect mean by ~1‰ relative to the bulk, accounting for much of the observed offset. Moreover, the 2.1‰ offset is well within the typical analytical accuracy of SIMS $\delta^{13}C$ measurements of extraterrestrial carbonates. The total $\delta^{13}C$ variation among extraterrestrial carbonates spans tens of per mille – for instance, inter-grain $\delta^{13}C$ variability exceeding 15-80‰ has been documented in CI, CM, and CR chondrites[63,69–71]– so a ~2‰ grain-average offset is insignificant in the context of the geological signals this protocol is designed to resolve. We conclude that our C isotope calibration is accurate within the combined analytical uncertainties, though a modest residual offset may partly reflect the spatial sampling bias inherent in comparing a linear transect average to a volume-weighted bulk value. We further note that the accuracy test on 10937 siderite ((Fe+Mn)# = 0.9), presented below, yields a smaller offset (0.8‰) at substantially higher (Fe+Mn)#, which is the compositional region where any hypothetical dead time artifact would be largest (see **Supplementary Information Section S5** for details). The fact that accuracy improves rather than degrades at high (Fe+Mn)# is inconsistent with a dead time artifact and supports the integrity of the parabolic calibration.

10937 Siderite

We analyzed $\delta^{13}C$ of 22 points across a single 10937 grain ((Fe+Mn)# = 0.9; **Table 1**) from mount 2, achieving internal error of ~2.1‰ (2SD) per analysis. Corrected $\delta^{13}C$ values varied from −10.7 ± 3.2‰ (2SD) to −15.4 ± 2.9‰ (2SD) (**Fig. 9b, Table 7**), reflecting a limited isotopic or thermal evolution of the parent fluid. The SD of all corrected $\delta^{13}C$ values is 1.3‰, which reflects isotopic homogeneity of this material.

The grain-average $\delta^{13}C$ value measured by SIMS was −13.9 ± 0.6‰ (2SE, n = 22), compared to the true grain-average $\delta^{13}C$ measured by phosphoric acid digestion of −13.1 ± 0.02‰ (2SE, n = 3) (**Fig. 9b, Tables 1, 7**). The offset between the two means is 0.8‰, which compares well to the 2SE of the SIMS mean and combined uncertainty of the two measurements propagated in quadrature (2SE=0.6‰, $\delta^{13}C$ offset/combined 2SE ~1.3) at 2SD level. This demonstrates that our C isotope calibration for magnesite-siderite series is accurate.

Ca isotopes

H884 Dolomite

We analyzed $\delta^{44}Ca$ of 29 points across the Fe-Mn zonation along a transect from Fe-poor to Fe-rich zones of an H884 grain from mount 2, achieving internal errors of ~0.2‰ (1SD) per analysis.

View Article Online
DOI: 10.1039/D6JA00136J

Across the (Fe+Mn)# range of 0.12-0.33, corrected δ^{44}Ca values varied from −0.84 ± 0.3‰ (1SD) to 2.3 ± 0.3‰ (1SD) (**Fig. 9c, Table 7**).

The grain-average δ^{44}Ca measured by SIMS was 0.66 ± 0.3‰ (2SE, n = 29), compared to the true grain-average δ^{44}Ca measured by MC-ICP-MS of 0.85 ± 0.1‰ (2SE, n = 3) (**Fig. 9c, Table 7**). The offset between the two means is 0.19‰, well within the combined uncertainty propagated in quadrature (2SE=0.3‰, δ^{44}Ca offset/combined uncertainty ~0.7), demonstrating that our Ca isotope calibration is accurate.

Mg isotopes

H884 Dolomite

We analyzed δ^{26}Mg of 20 points across the Fe, Mn zonation from two different grains in two different mounts, using two different calibrations within a single analytical session. We routinely achieved internal errors of ~0.2‰ (1SD) per analysis. The first grain from mount 1 showed relatively uniform (Fe+Mn)# (0.16-0.18), and corrected δ^{26}Mg values varied from −0.8 ± 0.4‰ (1SD) to 0.7 ± 0.5‰ (1SD) based on 7 analyses (**Fig. 9d, Table 8**). In the second grain from mount 2, (Fe+Mn)# varied from 0.12 to 0.27 across the Fe-zonation. From 13 measurements across this zonation, corrected δ^{26}Mg values varied from −1.8 ± 0.2‰ (1SD) to 1.5 ± 0.3‰ (1SD) (**Fig. 9d, Table 8**).

The grain-average δ^{26}Mg value measured by SIMS was −0.2 ± 0.4‰ (2SE, n = 20; comprising −0.16 ± 0.5‰ and −0.22 ± 0.5‰ for the first and second grains, respectively), compared to the true grain-average δ^{26}Mg measured by MC-ICP-MS of −0.5 ± 0.01‰ (2SE, n = 2) (**Fig. 9d, Table 8**). The offset between the two means is 0.3‰, within the combined uncertainty propagated in quadrature (2SE = 0.4‰, δ^{26}Mg offset/combined uncertainty ~ 0.75), demonstrating that our Mg isotope calibration is accurate.

MRR1077 and RK-1 Magnesites

We analyzed 3 points each on MRR1077 and RK-1 magnesite, with (Fe+Mn)# 0.01 and 0.06, respectively. Since these are compositionally uniform crystalline material (**Table 1**) that are isotopically homogeneous at the bulk scale (**Table 2**), it should be possible to test the accuracy of the method even with such small number of analyses.

The grain-average δ^{26}Mg values measured by SIMS were −1.23‰ and −1.21‰ for MRR1077 and RK-1 magnesite, respectively. Because n = 3 is too small for the normal approximation, we calculate the 95% confidence interval (CI) using the Student's t-test (for the three analyses, 95% CI = ±1.49‰ (MRR1077) and ±0.21‰ (RK-1 magnesite) for $t_{0.025,\,2} = 4.303$). The true grain-average δ^{26}Mg measured by MC-ICP-MS are −1.14 ± 0.08‰ (2SE, n = 2) and −0.88 ± 0.01‰ (2SE, n = 2) (**Fig. 9e, Table 2,8**). The offset between the two means (0.09‰ and 0.33‰) is within or near the 95% confidence intervals (±1.49‰ and ±0.21‰), so the SIMS-average and bulk values are statistically indistinguishable.

However, we note that the small number of analyses (n = 3) limits the statistical power of this test. With only 3 analyses, systematic offsets smaller than ~1.5‰ and ~0.2‰ cannot be conclusively detected at the 95% confidence level, including the mean offset between SIMS-average and bulk δ^{26}Mg values (upto 0.33‰). We therefore consider this result as preliminary evidence for the accuracy of our Mg isotope standardization. A more rigorous evaluation would require 8 or more analyses on this or additional secondary standards spanning a wider range of (Fe+Mn)#. Ideally, future work should include analyses of compositionally zoned Fe-bearing carbonates (like H884 test used for C, Mg, and Ca) to evaluate spot-level accuracy across the

View Article Online
DOI: 10.1039/D6JA00136J

calibration range. All SIMS-average δ^{26}Mg values agree with those from bulk MC-ICP-MS analyses within uncertainty and follow along a 1:1 line when plotted against each other (**Fig. 9e**), further validating our calibration.

Implications and future applications

Our study establishes IMF calibrations for coupled C-Mg-Ca isotope analysis of carbonates from the dolomite-ankerite and magnesite-siderite series at per mille or better precision (1SD) using a small-radius ion microprobe and demonstrates the accuracy of these calibrations using zoned secondary standards. The typical propagated uncertainties (1SD) are ~1.1‰ for δ^{13}C, 0.2-0.7‰ for δ^{26}Mg, and ~0.3‰ for δ^{44}Ca.

The range of δ^{13}C-$\delta^{25,26}$Mg-δ^{44}Ca of carbonates from terrestrial and meteoritic environments span several per mille[72–76], significantly larger than the analytical uncertainty of our protocol. Our method can therefore resolve carbonates formed under these distinct environmental conditions. Equilibrium C-Mg-Ca isotopic fractionations between carbonates and fluid also span several per mille at low temperatures (<~100°C) but diminish rapidly with increasing temperature[13,74,77,78]. Therefore, our standardization can be readily applied to investigate the origin of carbonates in low-temperature terrestrial and extraterrestrial environments, where isotopic fractionations exceed our analytical uncertainty. In higher-temperature systems, where isotopic fractionations are smaller, our precision may be insufficient to resolve subtle effects. Significantly better analytical precision can be achieved for δ^{13}C-$\delta^{25,26}$Mg-δ^{44}Ca analysis using large-radius instruments, which may help resolve minor isotope effects even at high-temperature settings and remains a tractable target for future studies.

Oxygen isotope IMF calibrations for dolomite-ankerite and magnesite-siderite minerals have been previously established[43,45]. The standard suite described here is compatible with those existing calibrations and can be used to add coupled C-Mg-Ca-O isotopic capability.

Conclusions

We have developed and characterized 22 carbonate reference materials (10 dolomite-ankerite, 11 magnesite-siderite, and 1 calcite) for *in situ* C-Mg-Ca isotope analysis by SIMS using a Cameca IMS 7f-GEO ion microprobe, and analyzed their matrix effects across multiple grain mounts, analytical sessions, and analytical conditions. Secondary ion yields (^{12}C, ^{24}Mg, ^{40}Ca) show systematic relationships with (Fe+Mn)# of carbonates, reflecting the competing effects of increasing electrical conductivity and decreasing elemental concentration as Fe+Mn substitution increases; depending on the isotopic system, these yields either gradually increase or define parabolic relationships with their Fe+Mn contents. For all isotope systems, IMF* spans tens of per mille and correlates strongly with (Fe+Mn)# of standards. For dolomite-ankerite minerals, over (Fe+Mn)# from 0 to 0.73, the ^{13}IMF*, ^{26}IMF*, and ^{44}IMF* span ranges of 5‰, 20‰, and 6‰, respectively, while for magnesite-siderite minerals over (Fe+Mn)# from 0 to 0.99, the ^{13}IMF* and ^{26}IMF*span ranges of 7‰ and 20‰, respectively. These matrix effects are well described by polynomial or sigmoidal functions ($R^2 \geq 0.92$), with calibration residuals averaging 0‰ and 1SD ≤0.7‰. Residuals show no correlation with (Fe+Mn)#, confirming that the empirical models adequately capture the IMF*-(Fe+Mn)# relationship and that secondary matrix-effect corrections are not necessary.

Using compositionally zoned secondary standards representative of carbonaceous chondrite carbonates, we demonstrate that these calibrations yield accurate isotopic compositions at the grain-average level within propagated uncertainties: ~2.2‰ (2SD) for C, 0.2-0.7‰ for Mg,

View Article Online
DOI: 10.1039/D6JA00136J

and ~0.3‰ for Ca. This work enables texture-resolved, coupled multi-isotope microanalysis of complex terrestrial and extraterrestrial carbonates, with immediate applications to samples from carbonaceous chondrites, asteroid return missions (Ryugu, Bennu), and Martian meteorites, where micron-scale chemical zoning and phyllosilicate association make bulk techniques unreliable. The calibrations presented here are specific to the Cameca IMS 7f-GEO at Caltech; laboratories using other instruments should develop independent calibrations, though the analytical framework and standard suite described here are transferable.

View Article Online
DOI: 10.1039/D6JA00136J

Author contributions: Conceptualization: SB, DSG; Methodology: SB, DSG, JAGW, CLB, TP, YG, MGS; Investigation: SB, JAGW, CLB; Formal analysis: SB; Visualization: SB; Validation: SB, DSG; Supervision: DSG; Funding acquisition: DSG; Project administration: DSG; Writing – original draft: SB, DSG; Writing – review & editing: SB, DSG, JAGW, CLB, YG.

Conflict of interest
The authors declare no competing interests.

Data availability
All data supporting this article are present in the paper and/or the Supplementary Information.

Acknowledgement
Michael Kipp and Rosa Grigoryan are thanked for helping us with the bulk Ca isotope analyses. We thank two anonymous reviewers for their thorough and constructive reviews, which helped us improve the clarity of this manuscript. This study was supported by startup provided by Yale University to D.S.G. Ca isotope analysis was performed at the Duke University Shared Materials Instrumentation Facility (SMIF) (RRID:SCR_027480), a member of the North Carolina Research Triangle Nanotechnology Network (RTNN), which is supported by the National Science Foundation (award number ECCS-2025064) as part of the National Nanotechnology Coordinated Infrastructure (NNCI).

View Article Online
DOI: 10.1039/D6JA00136J

References

1 P. K. Swart, *Sedimentology*, 2015, **62**, 1233–1304.
2 E. M. Stewart and J. J. Ague, *Nature Communications*, 2020, **11**, 6220.
3 L. H. Tanner, *Developments in Sedimentology*, 2010, **62**, 179–214.
4 T. E. Cerling, *Earth and Planetary science letters*, 1984, **71**, 229–240.
5 G. Jiang, M. J. Kennedy and N. Christie-Blick, *Nature*, 2003, **426**, 822–826.
6 P. Ghosh, C. N. Garzione and J. M. Eiler, *Science*, 2006, **311**, 511–515.
7 J. M. Eiler, *Quaternary Science Reviews*, 2011, **30**, 3575–3588.
8 J. A. Wostbrock, U. Brand, T. B. Coplen, P. K. Swart, S. J. Carlson, A. J. Brearley and Z. D. Sharp, *Geochimica et Cosmochimica Acta*, 2020, **288**, 369–388.
9 E. L. Scheller, C. Swindle, J. Grotzinger, H. Barnhart, S. Bhattacharjee, B. L. Ehlmann, K. Farley, W. W. Fischer, R. Greenberger and M. Ingalls, *Journal of Geophysical Research: Planets*, 2021, **126**, e2021JE006828.
10 C. Swindle, P. Vasconcelos, Z. Dimarco, N. Dalleska, A. Nguyen, E. Cardarelli, S. Bhattacharjee, K. Farley and T. Present, *Chemical Geology*, 2025, 123068.
11 A. Brewer, F.-Z. Teng and D. Dethier, *chemical Geology*, 2018, **501**, 95–103.
12 J. C. de Obeso, D. P. Santiago Ramos, J. A. Higgins and P. B. Kelemen, *Journal of Geophysical Research: Solid Earth*, 2021, **126**, e2020JB020237.
13 S. Bhattacharjee, A. S. Patel, J. Cheng, M. J. Raudsepp, S. Wilson, W. A. Goddard, P. D. Asimow and J. M. Eiler, *Geochimica et Cosmochimica Acta*, 2025, **409**, 212–229.
14 J. A. Higgins and D. P. Schrag, *Geochimica et Cosmochimica Acta*, 2010, **74**, 5039–5053.
15 D. Lemarchand, G. J. Wasserburg and D. A. Papanastassiou, *Geochimica et cosmochimica acta*, 2004, **68**, 4665–4678.
16 N. Gussone, F. Böhm, A. Eisenhauer, M. Dietzel, A. Heuser, B. M. Teichert, J. Reitner, G. Wörheide and W.-C. Dullo, *Geochimica et Cosmochimica Acta*, 2005, **69**, 4485–4494.
17 C. L. Blättler, W.-L. Hong, K. Kirsimäe, J. A. Higgins and A. Lepland, *Geochimica et Cosmochimica Acta*, 2021, **298**, 227–239.
18 C. Cao, X.-M. Liu, C. P. Bataille and C. Liu, *Chemical Geology*, 2020, **532**, 119413.
19 C. Swindle, P. Vasconcelos, N. Dalleska, E. Cardarelli, S. Bhattacharjee, Z. Dimarco, K. A. Farley and T. Present, *Applied Geochemistry*, 2025, **191**, 106494.
20 A. H. Treiman, H. E. Amundsen, D. F. Blake and T. Bunch, *Earth and Planetary Science Letters*, 2002, **204**, 323–332.
21 J. W. Valley, J. M. Eiler, C. M. Graham, E. K. Gibson, C. S. Romanek and E. M. Stolper, *Science*, 1997, **275**, 1633–1638.
22 C. E. Moyano-Cambero, J. M. Trigo-Rodríguez, M. I. Benito, J. Alonso-Azcárate, M. R. Lee, N. Mestres, M. Martínez-Jiménez, F. J. Martín-Torres and J. Fraxedas, *Meteorit & Planetary Scien*, 2017, **52**, 1030–1047.
23 T. Nakamura, M. Matsumoto, K. Amano, Y. Enokido, M. E. Zolensky, T. Mikouchi, H. Genda, S. Tanaka, M. Y. Zolotov, K. Kurosawa, S. Wakita, R. Hyodo, H. Nagano, D. Nakashima, Y. Takahashi, Y. Fujioka, M. Kikuiri, E. Kagawa, M. Matsuoka, A. J. Brearley, A. Tsuchiyama, M. Uesugi, J. Matsuno, Y. Kimura, M. Sato, R. E. Milliken, E. Tatsumi, S. Sugita, T. Hiroi, K. Kitazato, D. Brownlee, D. J. Joswiak, M. Takahashi, K. Ninomiya, T. Takahashi, T. Osawa, K. Terada, F. E. Brenker, B. J. Tkalcec, L. Vincze, R. Brunetto, A. Aléon-Toppani, Q. H. S. Chan, M. Roskosz, J.-C. Viennet, P. Beck, E. E. Alp, T. Michikami, Y. Nagaashi, T. Tsuji, Y. Ino, J. Martinez, J. Han, A. Dolocan, R. J. Bodnar, M. Tanaka, H. Yoshida, K. Sugiyama, A. J. King, K. Fukushi, H. Suga, S. Yamashita, T. Kawai, K. Inoue, A.

View Article Online
DOI: 10.1039/D6JA00136J

Nakato, T. Noguchi, F. Vilas, A. R. Hendrix, C. Jaramillo-Correa, D. L. Domingue, G. Dominguez, Z. Gainsforth, C. Engrand, J. Duprat, S. S. Russell, E. Bonato, C. Ma, T. Kawamoto, T. Wada, S. Watanabe, R. Endo, S. Enju, L. Riu, S. Rubino, P. Tack, S. Takeshita, Y. Takeichi, A. Takeuchi, A. Takigawa, D. Takir, T. Tanigaki, A. Taniguchi, K. Tsukamoto, T. Yagi, S. Yamada, K. Yamamoto, Y. Yamashita, M. Yasutake, K. Uesugi, I. Umegaki, I. Chiu, T. Ishizaki, S. Okumura, E. Palomba, C. Pilorget, S. M. Potin, A. Alasli, S. Anada, Y. Araki, N. Sakatani, C. Schultz, O. Sekizawa, S. D. Sitzman, K. Sugiura, M. Sun, E. Dartois, E. De Pauw, Z. Dionnet, Z. Djouadi, G. Falkenberg, R. Fujita, T. Fukuma, I. R. Gearba, K. Hagiya, M. Y. Hu, T. Kato, T. Kawamura, M. Kimura, M. K. Kubo, F. Langenhorst, C. Lantz, B. Lavina, M. Lindner, J. Zhao, B. Vekemans, D. Baklouti, B. Bazi, F. Borondics, S. Nagasawa, G. Nishiyama, K. Nitta, J. Mathurin, T. Matsumoto, I. Mitsukawa, H. Miura, A. Miyake, Y. Miyake, H. Yurimoto, R. Okazaki, H. Yabuta, H. Naraoka, K. Sakamoto, S. Tachibana, H. C. Connolly, D. S. Lauretta, M. Yoshitake, M. Yoshikawa, K. Yoshikawa, K. Yoshihara, Y. Yokota, K. Yogata, H. Yano, Y. Yamamoto, D. Yamamoto, M. Yamada, T. Yamada, T. Yada, K. Wada, T. Usui, R. Tsukizaki, F. Terui, H. Takeuchi, Y. Takei, A. Iwamae, H. Soejima, K. Shirai, Y. Shimaki, H. Senshu, H. Sawada, T. Saiki, M. Ozaki, G. Ono, T. Okada, N. Ogawa, K. Ogawa, R. Noguchi, H. Noda, M. Nishimura, N. Namiki, S. Nakazawa, T. Morota, A. Miyazaki, A. Miura, Y. Mimasu, K. Matsumoto, K. Kumagai, T. Kouyama, S. Kikuchi, K. Kawahara, S. Kameda, T. Iwata, Y. Ishihara, M. Ishiguro, H. Ikeda, S. Hosoda, R. Honda, C. Honda, Y. Hitomi, N. Hirata, N. Hirata, T. Hayashi, M. Hayakawa, K. Hatakeda, S. Furuya, R. Fukai, A. Fujii, Y. Cho, M. Arakawa, M. Abe, S. Watanabe and Y. Tsuda, *Science*, 2023, **379**, eabn8671.

24 D. S. Lauretta, H. C. Connolly, J. E. Aebersold, C. M. O. Alexander, R. Ballouz, J. J. Barnes, H. C. Bates, C. A. Bennett, L. Blanche, E. H. Blumenfeld, S. J. Clemett, G. D. Cody, D. N. DellaGiustina, J. P. Dworkin, S. A. Eckley, D. I. Foustoukos, I. A. Franchi, D. P. Glavin, R. C. Greenwood, P. Haenecour, V. E. Hamilton, D. H. Hill, T. Hiroi, K. Ishimaru, F. Jourdan, H. H. Kaplan, L. P. Keller, A. J. King, P. Koefoed, M. K. Kontogiannis, L. Le, R. J. Macke, T. J. McCoy, R. E. Milliken, J. Najorka, A. N. Nguyen, M. Pajola, A. T. Polit, K. Righter, H. L. Roper, S. S. Russell, A. J. Ryan, S. A. Sandford, P. F. Schofield, C. D. Schultz, L. B. Seifert, S. Tachibana, K. L. Thomas-Keprta, M. S. Thompson, V. Tu, F. Tusberti, K. Wang, T. J. Zega, C. W. V. Wolner, and the OSIRIS-REx Sample Analysis Team, *Meteorit & Planetary Scien*, 2024, **59**, 2453–2486.

25 E. Zinner^1, *New frontiers in stable isotopic research: laser probes, ion probes, and small-sample analysis*, 1989, 145.

26 C. R. Neal, J. P. Davidson and K. D. McKeegan, *Reviews of Geophysics*, 1995, **33**, 25–32.

27 J. W. Valley and N. T. Kita, .

28 R. L. Hervig, P. Williams, R. M. Thomas, S. N. Schauer and I. M. Steele, *International Journal of Mass Spectrometry and Ion Processes*, 1992, **120**, 45–63.

29 J. M. Eiler, C. Graham and J. W. Valley, *Chemical Geology*, 1997, **138**, 221–244.

30 C. Rollion-Bard and J. Marin-Carbonne, *Journal of Analytical Atomic Spectrometry*, 2011, **26**, 1285–1289.

31 J. Isa, I. E. Kohl, M.-C. Liu, J. T. Wasson, E. D. Young and K. D. McKeegan, *Chemical Geology*, 2017, **458**, 14–21.

32 K. Fukuda, B. L. Beard, D. R. Dunlap, M. J. Spicuzza, J. H. Fournelle, M. Wadhwa and N. T. Kita, *Chemical geology*, 2020, **540**, 119482.

33 K. A. McCain, M.-C. Liu and K. D. McKeegan, *Journal of Vacuum Science & Technology B*.

View Article Online
DOI: 10.1039/D6JA00136J

34 J.-Y. Xu, Q.-L. Li, G.-Q. Tang, K. Lu, Y. Liu, L.-J. Feng and J. C. Melgarejo, *Anal. Chem.*, 2022, **94**, 7944–7951.
35 I. C. Fitzsimons, B. Harte and R. M. Clark, *Mineralogical Magazine*, 2000, **64**, 59–83.
36 J. M. Huberty, N. T. Kita, R. Kozdon, P. R. Heck, J. H. Fournelle, M. J. Spicuzza, H. Xu and J. W. Valley, *Chemical Geology*, 2010, **276**, 269–283.
37 N. T. Kita, J. M. Huberty, R. Kozdon, B. L. Beard and J. W. Valley, *Surface & Interface Analysis*, 2011, **43**, 427–431.
38 M. Endreß and A. Bischoff, *Geochimica et Cosmochimica Acta*, 1996, **60**, 489–507.
39 M. E. Tucker and V. P. Wright, *Carbonate sedimentology*, John Wiley & Sons, 2009.
40 M. R. Lee, C. M. O. Alexander, A. Bischoff, A. J. Brearley, E. Dobrică, W. Fujiya, C. Le Guillou, A. J. King, E. Van Kooten, A. N. Krot, J. Leitner, Y. Marrocchi, M. Patzek, M. I. Petaev, L. Piani, O. Pravdivtseva, L. Remusat, M. Telus, A. Tsuchiyama and L. G. Vacher, *Space Sci Rev*, 2025, **221**, 11.
41 J. M. Eiler, J. W. Valley and C. M. Graham, in *Conference Paper, 28th Annual Lunar and Planetary Science Conference, p. 327.*, 1997, vol. 28, p. 327.
42 L. A. Leshin, K. D. McKeegan, P. K. Carpenter and R. P. Harvey, *Geochimica et Cosmochimica Acta*, 1998, **62**, 3–13.
43 M. G. Śliwiński, K. Kitajima, R. Kozdon, M. J. Spicuzza, J. H. Fournelle, A. Denny and J. W. Valley, *Geostandard Geoanalytic Res*, 2016, **40**, 157–172.
44 M. G. Śliwiński, K. Kitajima, R. Kozdon, M. J. Spicuzza, J. H. Fournelle, A. Denny and J. W. Valley, *Geostandard Geoanalytic Res*, 2016, **40**, 173–184.
45 M. G. Śliwiński, K. Kitajima, M. J. Spicuzza, I. J. Orland, A. Ishida, J. H. Fournelle and J. W. Valley, *Geostandards and Geoanalytical Research*, 2018, **42**, 49–76.
46 C. Rollion-Bard, N. Vigier and S. Spezzaferri, *Chemical Geology*, 2007, **244**, 679–690.
47 M. K. Azer, H. A. Gahlan, P. D. Asimow, H. S. Mubarak and K. M. Al-Kahtany, *The Journal of Geology*, 2019, **127**, 81–107.
48 P. K. Swart, S. J. Burns and J. J. Leder, *Chemical Geology: Isotope Geoscience Section*, 1991, **86**, 89–96.
49 N. M. Mammone, Master's Thesis, University of California, Riverside, 2021.
50 R. N. Bryant, T. M. Present, A.-S. C. Ahm, H.-L. O. McClelland, D. Razionale and C. L. Blättler, *Geochimica et Cosmochimica Acta*, 2022, **328**, 1–18.
51 S. Riechelmann, V. Mavromatis, D. Buhl, M. Dietzel, R. Hoffmann, N. Jöns, I. Kell-Duivestein and A. Immenhauser, *Geochimica et Cosmochimica Acta*, 2018, **235**, 333–359.
52 F. L. Tissot, D. Cleveland, R. Grigoryan, M. A. Kipp, R. T. Shafiee, E. Miaou, R. Chunduri, H. Melton, T. Tacail and D. Razionale, *Metallomics*, 2024, **16**, mfae050.
53 R. Grigoryan, W. Swenson, M. P. Field, M. C. De Silva, A. Strasma, N. Jayasundara and M. A. Kipp, *Anal Bioanal Chem*, 2026, **418**, 1497–1510.
54 D. Hippler, A. Schmitt, N. Gussone, A. Heuser, P. Stille, A. Eisenhauer and T. F. Nägler, *Geostandards Newsletter*, 2003, **27**, 13–19.
55 F. Z. Page, N. T. Kita and J. W. Valley, *Chemical Geology*, 2010, **270**, 9–19.
56 A. Vho, D. Rubatto, B. Putlitz and A. Bouvier, *Geostandard Geoanalytic Res*, 2020, **44**, 459–471.
57 D. Vielzeuf, M. Champenois, J. W. Valley, F. Brunet and J. L. Devidal, *Chemical Geology*, 2005, **223**, 208–226.
58 R. B. Ickert and R. A. Stern, *Geostandards and Geoanalytical Research*, 2013, **37**, 429–448.
59 L. M. Anovitz and E. J. Essene, *Journal of Petrology*, 1987, **28**, 389–415.

View Article Online
DOI: 10.1039/D6JA00136J

60 E. Franzolin, M. W. Schmidt and S. Poli, *Contributions to Mineralogy and Petrology*, 2011, **161**, 213–227.
61 N. T. Kita, K. Kitajima, K. Nagashima, N. Kawasaki, N. Sakamoto, W. Fujiya, Y. Abe, J. Aléon, C. M. O. Alexander, S. Amari, Y. Amelin, K. Bajo, M. Bizzarro, A. Bouvier, R. W. Carlson, M. Chaussidon, B. Choi, N. Dauphas, A. M. Davis, T. Di Rocco, R. Fukai, I. Gautam, M. K. Haba, Y. Hibiya, H. Hidaka, H. Homma, P. Hoppe, G. R. Huss, K. Ichida, T. Iizuka, T. R. Ireland, A. Ishikawa, S. Itoh, T. Kleine, S. Komatani, A. N. Krot, M. Liu, Y. Masuda, K. D. McKeegan, M. Morita, K. Motomura, F. Moynier, I. Nakai, A. Nguyen, L. Nittler, M. Onose, A. Pack, C. Park, L. Piani, L. Qin, S. S. Russell, M. Schönbächler, L. Tafla, H. Tang, K. Terada, Y. Terada, T. Usui, S. Wada, M. Wadhwa, R. J. Walker, K. Yamashita, Q. Yin, T. Yokoyama, S. Yoneda, E. D. Young, H. Yui, A. Zhang, T. Nakamura, H. Naraoka, T. Noguchi, R. Okazaki, K. Sakamoto, H. Yabuta, M. Abe, A. Miyazaki, A. Nakato, M. Nishimura, T. Okada, T. Yada, K. Yogata, S. Nakazawa, T. Saiki, S. Tanaka, F. Terui, Y. Tsuda, S. Watanabe, M. Yoshikawa, S. Tachibana and H. Yurimoto, *Meteorit & Planetary Scien*, 2024, **59**, 2097–2116.
62 C. A. Johnson and M. Prinz, *Geochimica et Cosmochimica Acta*, 1993, **57**, 2843–2852.
63 W. Fujiya, N. Kawasaki, K. Nagashima, N. Sakamoto, C. M. O'D. Alexander, N. T. Kita, K. Kitajima, Y. Abe, J. Aléon and S. Amari, *Nature Geoscience*, 2023, **16**, 675–682.
64 K. Itano, K. Fukuda, N. T. Kita, K. Ueki, T. Kuwatani and S. Akaho, *Rapid Comm Mass Spectrometry*, 2025, **39**, e10038.
65 M. S. Fantle and J. Higgins, *Geochimica et Cosmochimica Acta*, 2014, **142**, 458–481.
66 L. A. Martin, D. Rubatto, C. Crépisson, J. Hermann, B. Putlitz and A. Vitale-Brovarone, *Chemical Geology*, 2014, **374**, 25–36.
67 M. D. Suttle, A. J. King, P. F. Schofield, H. Bates and S. S. Russell, *Geochimica et Cosmochimica Acta*, 2021, **299**, 219–256.
68 J. M. Eiler, J. W. Valley, C. M. Graham and J. Fournelle, *Geochimica et Cosmochimica Acta*, 2002, **66**, 1285–1303.
69 K. A. McCain, N. Matsuda, M.-C. Liu, K. D. McKeegan, A. Yamaguchi, M. Kimura, N. Tomioka, M. Ito, N. Imae and M. Uesugi, *Nature Astronomy*, 2023, **7**, 309–317.
70 C. M. O. Alexander, R. Bowden, M. L. Fogel and K. T. Howard, *Meteorit & Planetary Scien*, 2015, **50**, 810–833.
71 A. Bischoff, C. M. Alexander, J.-A. Barrat, C. Burkhardt, H. Busemann, D. Degering, T. Di Rocco, M. Fischer, T. Fockenberg and D. I. Foustoukos, *Geochimica et Cosmochimica Acta*, 2021, **293**, 142–186.
72 M. Schidlowski, *Annual Review of Earth and Planetary Sciences, Vol. 15, p. 47*, 1987, **15**, 47.
73 F.-Z. Teng, *Reviews in Mineralogy and Geochemistry*, 2017, **82**, 219–287.
74 N. Gussone, A.-D. Schmitt, A. Heuser, F. Wombacher, M. Dietzel, E. Tipper and M. Schiller, *Calcium Stable Isotope Geochemistry*, Springer Berlin Heidelberg, Berlin, Heidelberg, 2016.
75 B. L. Beard and C. M. Johnson, *Reviews in Mineralogy and Geochemistry*, 2004, **55**, 319–357.
76 N. Dauphas, S. G. John and O. Rouxel, *Rev. Mineral. Geochem*, 2017, **82**, 415–510.
77 R. A. Wiesli, B. L. Beard and C. M. Johnson, *Chemical Geology*, 2004, **211**, 343–362.
78 A. Immenhauser, D. Buhl, D. Richter, A. Niedermayr, D. Riechelmann, M. Dietzel and U. Schulte, *Geochimica et Cosmochimica Acta*, 2010, **74**, 4346–4364.

View Article Online
DOI: 10.1039/D6JA00136J

Figures and Tables

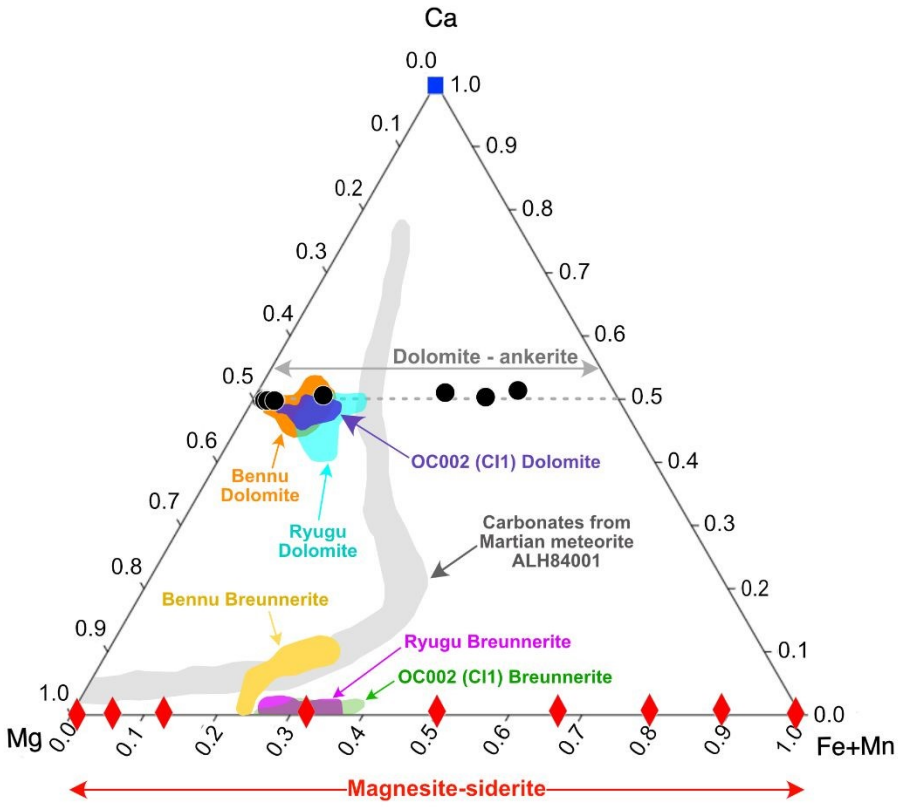

Figure 1: Major cation compositions of carbonate standards (calcite: blue square; dolomite–ankerite: black circles; magnesite-siderite: red diamonds) plotted on a Ca-Mg-(Fe+Mn) ternary diagram. Fields for selected extraterrestrial carbonates are shown for comparison: ALH84001 (gray band), Ryugu dolomites and breunnerites (sky blue and purple fields, respectively), and Bennu dolomites and breunnerites (orange and yellow fields, respectively).

View Article Online
DOI: 10.1039/D6JA00136J

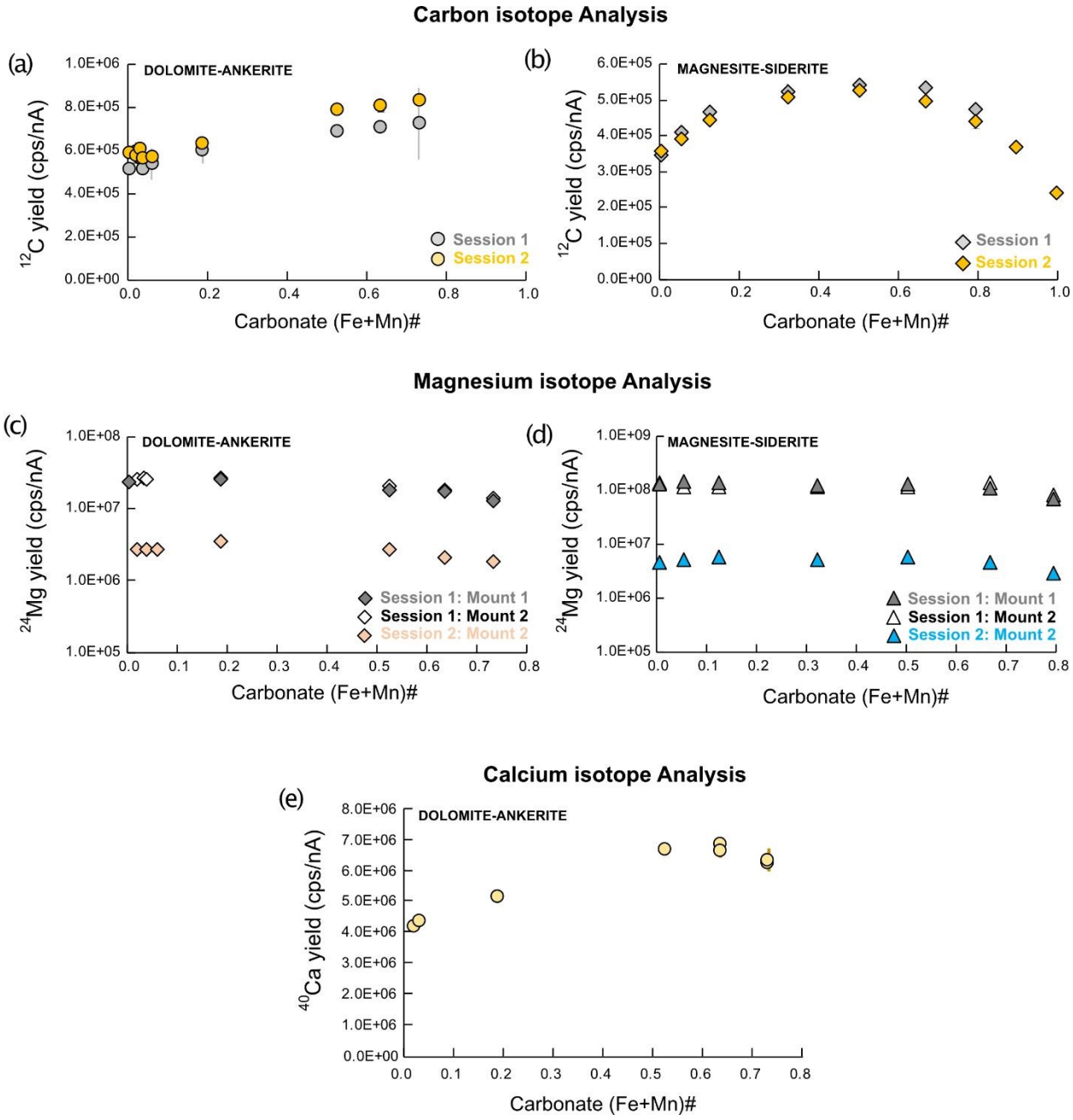

Figure 2: Secondary ion yield as a function of (Fe+Mn)# for carbonate standards. (**a**) ^{12}C yield, dolomite-ankerite. (**b**) ^{12}C yield, magnesite–siderite. (**c**) ^{24}Mg yield, dolomite-ankerite. (**d**) ^{24}Mg yield, magnesite-siderite. (**e**) ^{40}Ca yield, dolomite-ankerite. Different sessions and mounts are distinguished by symbol fill as indicated in the legend. Error bars are 1SD. Note that vertical axes for panels c, d are in logarithmic scale.

View Article Online
DOI: 10.1039/D6JA00136J

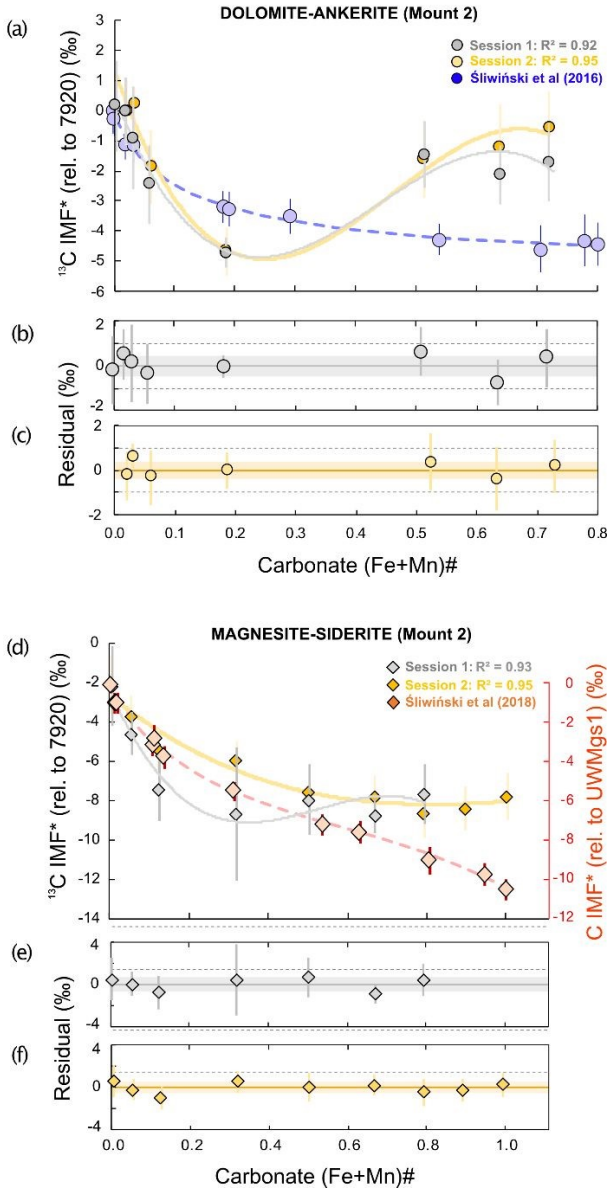

Figure 3: ^{13}IMF* as a function of (Fe+Mn)# for carbon isotope analysis. (**a**) Dolomite-ankerite minerals; session 1 (gray circles) and session 2 (yellow circles) with polynomial fits (solid lines; R^2 = 0.92 and 0.95, respectively). ^{13}IMF*-(Fe+Mn)# evaluated using a large radius SIMS from a previous study[44] is shown for reference (purple circles, blue dotted line is best fit, error bars: 2SE propagated). (**b,c**) Calibration residuals for sessions 1 and 2, respectively; solid lines show the mean and shaded areas the 1SD envelope. (**d**) Magnesite-siderite minerals; session 1 (gray diamonds) and session 2 (yellow diamonds) with polynomial fits (R^2 = 0.93 and 0.95, respectively). ^{13}IMF*-(Fe+Mn)# evaluated using a large radius SIMS from a previous study[45] is shown for reference (orange diamonds, orange dotted line is best fit; error bars: 2SE propagated). (**e,f**) Calibration residuals for sessions 1 and 2, respectively. Error bars are 1SD propagated.

View Article Online
DOI: 10.1039/D6JA00136J

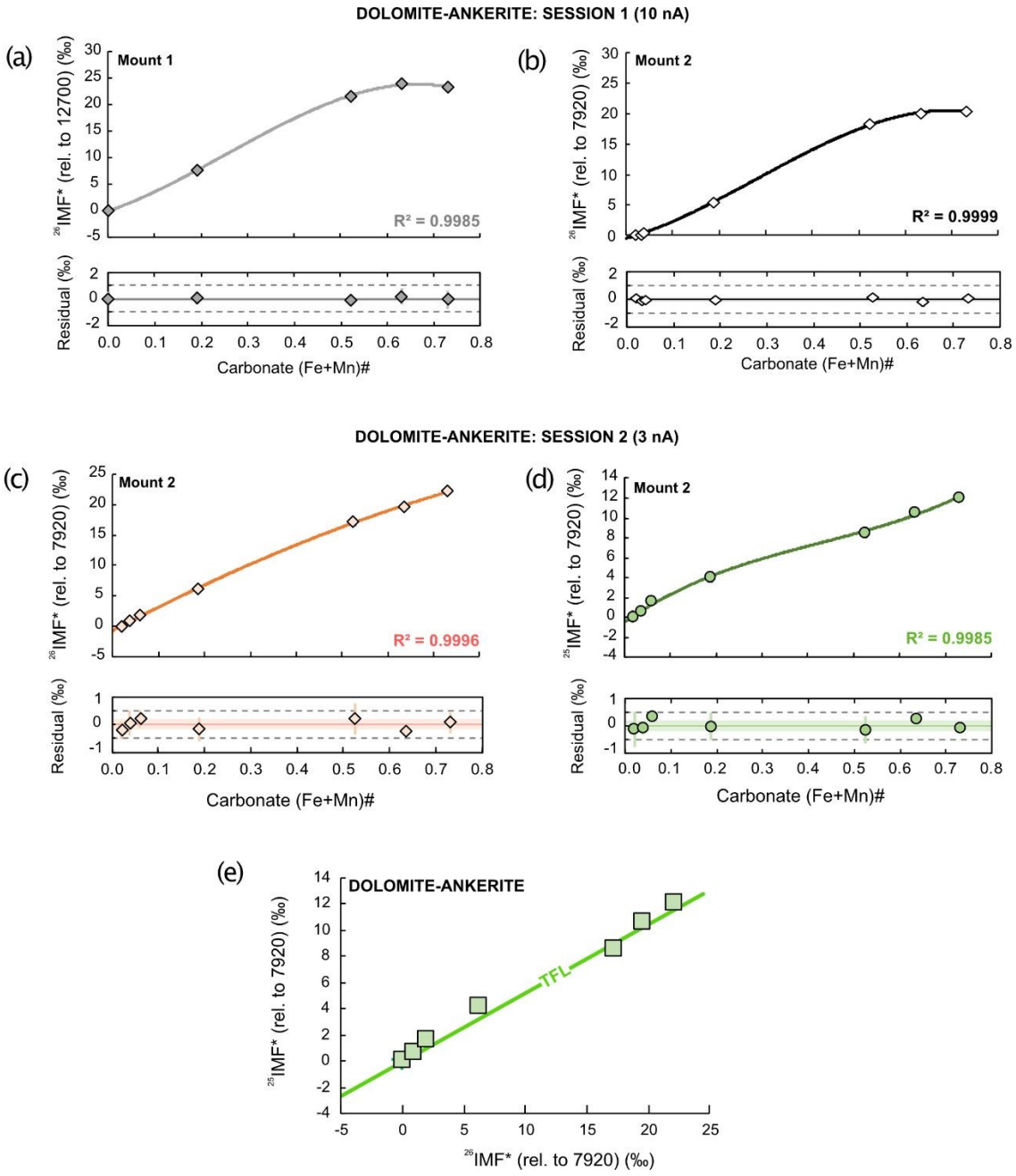

Figure 4: ^{26,25}IMF* as a function of (Fe+Mn)# for Mg isotope analysis of dolomite–ankerite minerals. (**a-d**) Upper panels show IMF* with polynomial fits ($R^2 \geq 0.998$); lower panels show calibration residuals (solid lines = mean, shaded areas = 1SD). (**a**) ^{26}IMF*, mount 1, session 1. (**b**) ^{26}IMF*, mount 2, session 1. (**c**) ^{26}IMF*, mount 2, session 2. (**d**) ^{25}IMF*, mount 2, session 2. (**e**) ^{26}IMF* vs. ^{25}IMF*, confirming terrestrial mass-dependent fractionation. Error bars are 1SD propagated and often smaller than symbols.

View Article Online
DOI: 10.1039/D6JA00136J

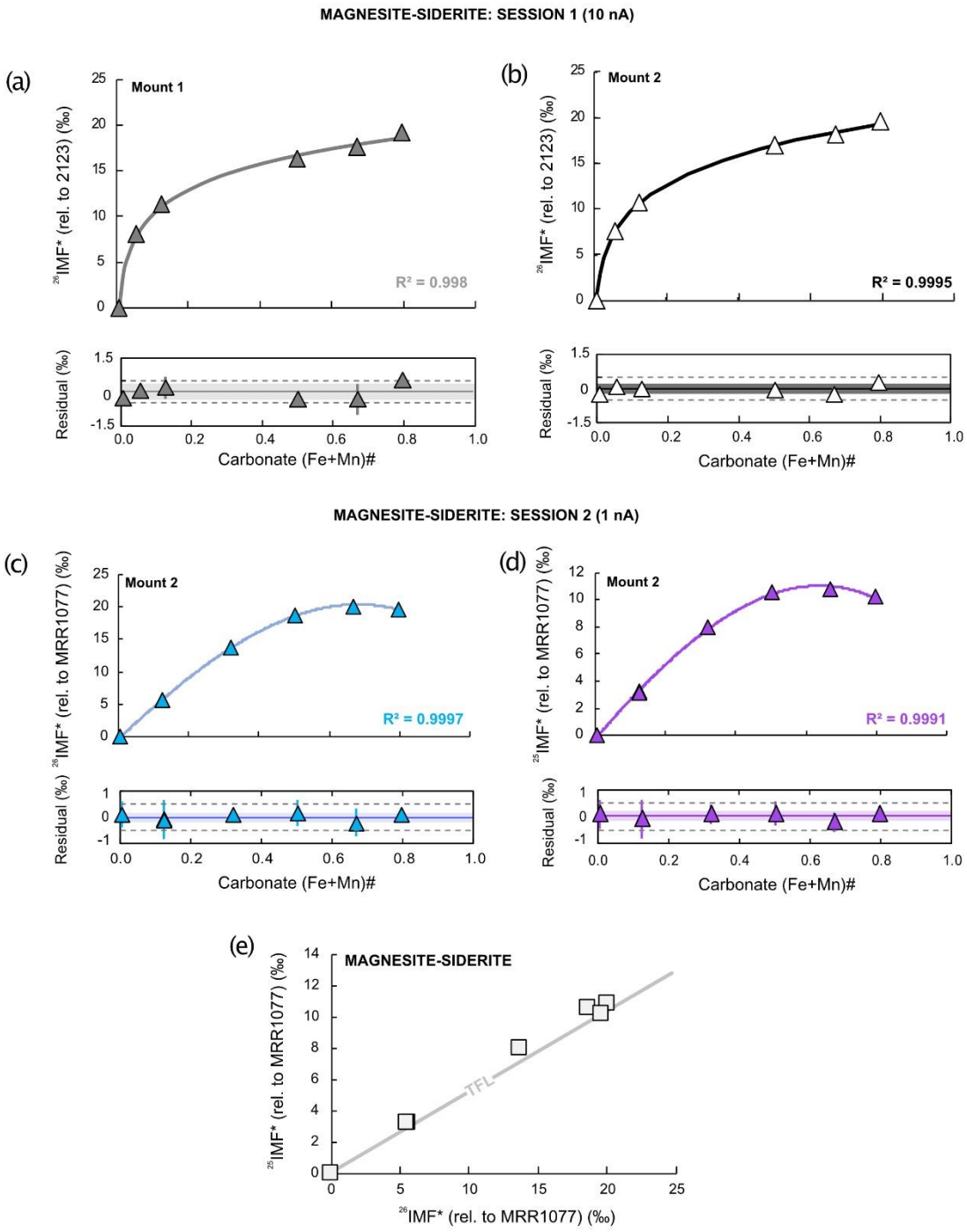

Figure 5: ^{26,25}IMF* as a function of (Fe+Mn)# for Mg isotope analysis of magnesite-siderite minerals. (**a-d**) Upper panels show IMF* with fitted curves (R^2 ≥0.998); lower panels show calibration residuals (solid lines = mean, shaded areas = 1SD). (**a**) ^{26}IMF*, mount 1, session 1 (sigmoidal fit). (**b**) ^{26}IMF*, mount 2, session 1 (sigmoidal fit). (**c**) ^{26}IMF*, mount 2, session 2 (polynomial fit). (**d**) ^{25}IMF*, mount 2, session 2 (polynomial fit). (**e**) ^{26}IMF* vs. ^{25}IMF*, confirming terrestrial mass-dependent fractionation. Error bars are 1SD propagated and often smaller than symbols.

View Article Online
DOI: 10.1039/D6JA00136J

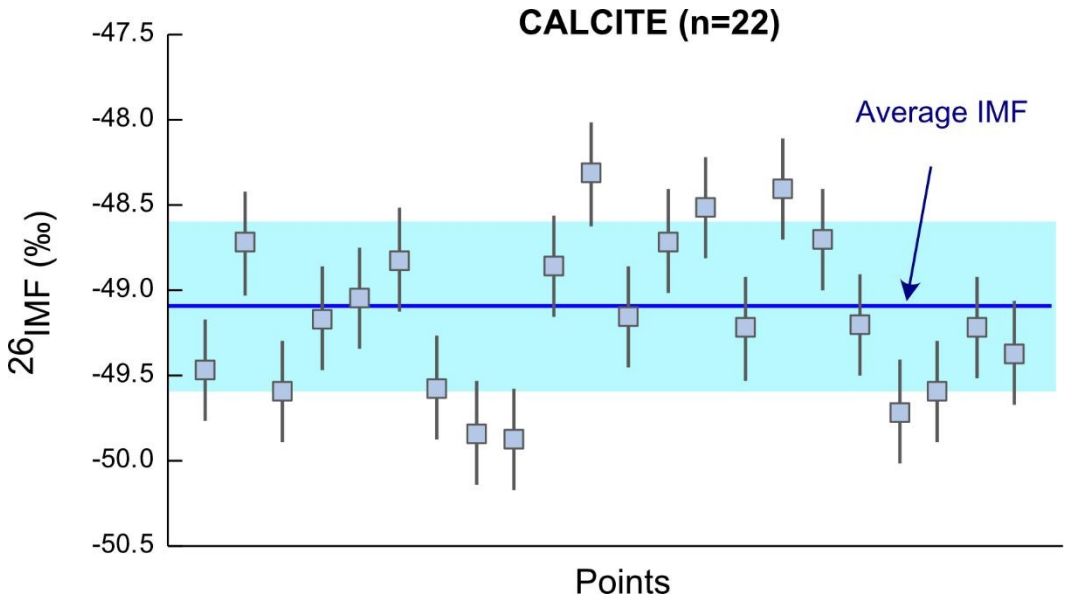

Figure 6: Absolute ^{26}IMF for Mg isotope analysis of calcite. Each point represents an individual SIMS analysis. Blue line and shaded region show the mean (−49.1‰) and 1SD (±0.46‰), respectively. Error bars are 1SD propagated.

View Article Online
DOI: 10.1039/D6JA00136J

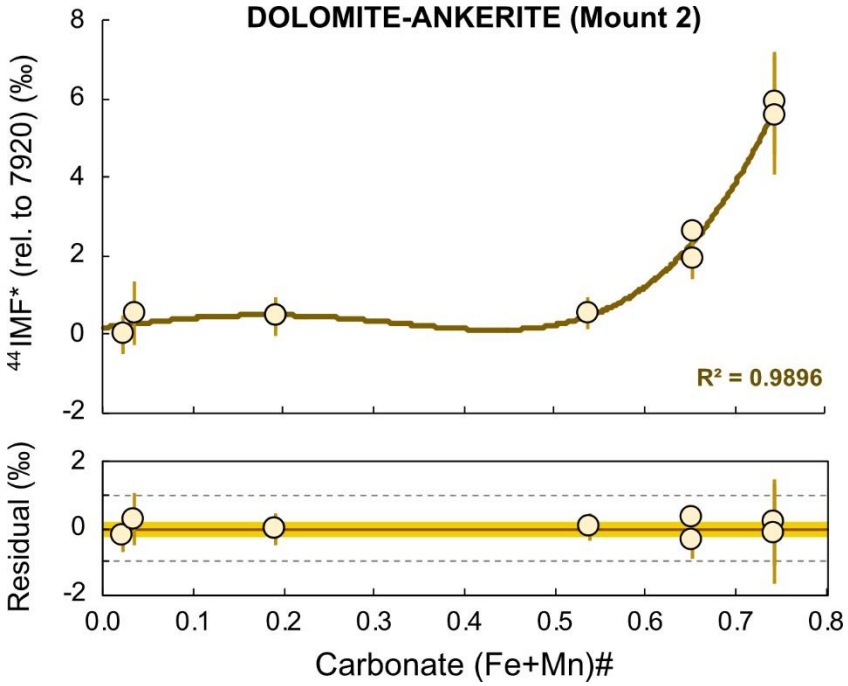

Figure 7: ^{44}IMF* as a function of (Fe+Mn)# for Ca isotope analysis of dolomite–ankerite minerals. Upper panel: ^{44}IMF* (yellow circles) with fourth-order polynomial fit (brown line; $R^2 = 0.989$). Lower panel: calibration residuals (brown line = mean, yellow shaded area = 1SD). Error bars are 1SD propagated.

View Article Online
DOI: 10.1039/D6JA00136J

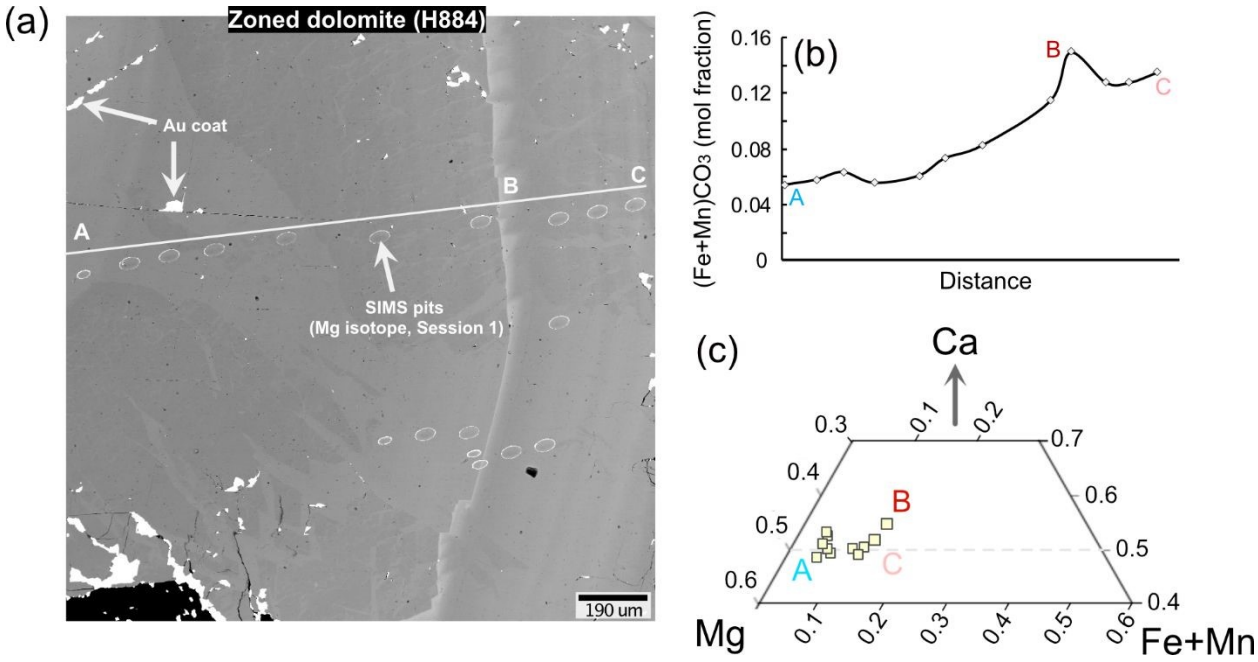

Figure 8: Chemical composition of zoned dolomite H884. (**a**) Backscattered electron (BSE) image of a H884 dolomite grain from mount 2, showing zoning patterns as alternate light and dark regions. Elliptical SIMS pits from Mg isotope analysis from session 1 are marked. Scale bar is 190 µm. (**b**) Electron microprobe analysis revealed a large variation in $FeCO_3$+$MnCO_3$ content (mol fraction) of carbonates along the transect A-B-C (solid white line in panel a). (**c**) Composition of these spots in Ca-Mg-(Fe+Mn) ternary. Gray dotted line indicates dolomite-ankerite join.

View Article Online
DOI: 10.1039/D6JA00136J

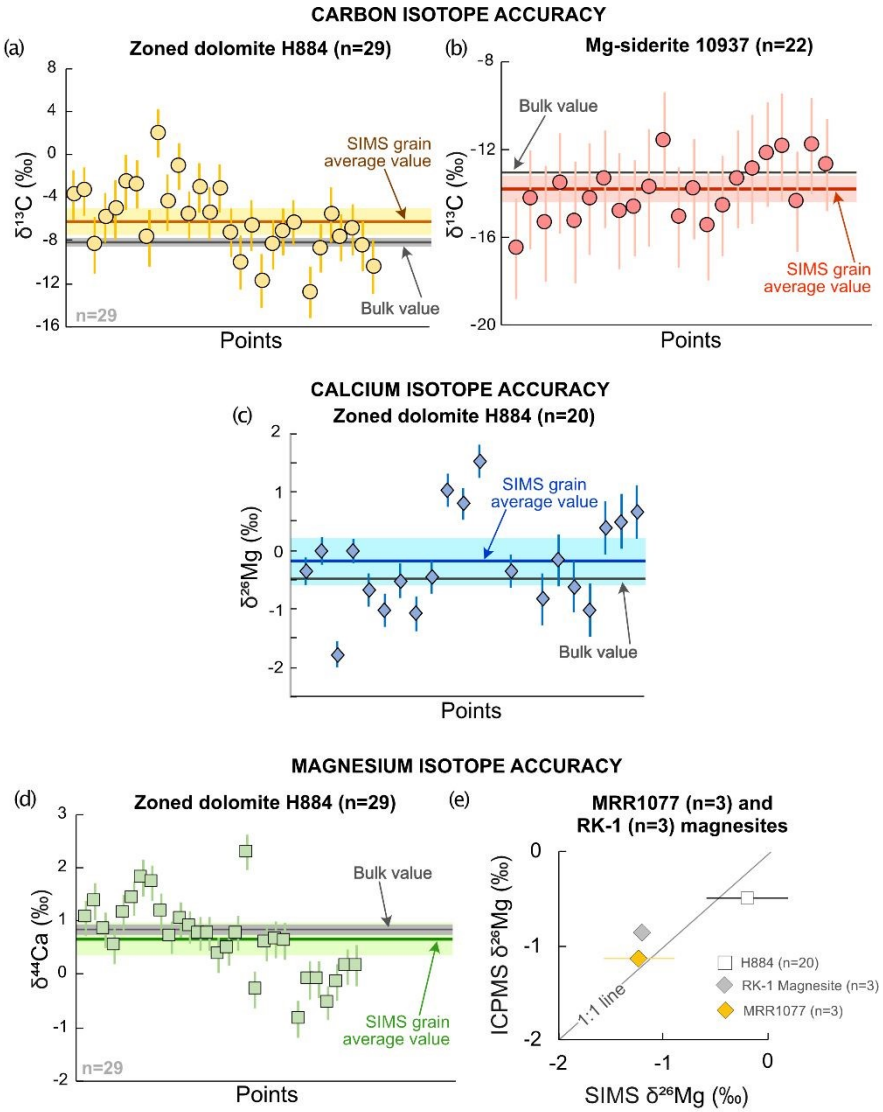

Figure 9: Accuracy test results: corrected SIMS isotope ratios compared with independent bulk measurements. (**a**) $\delta^{13}C$ of H884 dolomite across chemical zonation. (**b**) $\delta^{13}C$ across 10937 siderite grain. (**c**) $\delta^{44}Ca$ of H884 dolomite across chemical zonation. (**d**) $\delta^{26}Mg$ of H884 dolomite across chemical zonation. In panels **a-d**, total number of spots analyzed (n) from each mineral is indicated in the caption. Colored lines and shaded regions show the SIMS grain-average and 2SE, while black lines and gray shading show the true bulk value and 2SE. Error bars are 2SD propagated for $\delta^{13}C$ and 1SD propagated for all other systems. Grain-average SIMS compositions agree with bulk values within analytical uncertainty in all cases. (**e**) Comparison of SIMS grain-average $\delta^{26}Mg$ of chemically homogeneous magnesites (RK-1, MRR1077) and zoned dolomite (H884) with bulk MC-ICP-MS values, with solid black line showing 1:1 agreement. Error bars are 2SE propagated, and number of spots analyzed (n) for each mineral is shown in legend.

Table 1: Major cation composition (in mol fraction of respective end member carbonate) of carbonate standards determined by wavelength-dispersive X-ray spectroscopy (WDS) using an electron microprobe.

Name	n_EPMA	$MgCO_3$ (mol fraction)	1SD	1SE	$CaCO_3$ (mol fraction)	1SD	1SE	$FeCO_3$ (mol fraction)	1SD	1SE	$MnCO_3$ (mol fraction)	1SD	1SE	(Fe+Mn)#	1SE
Primary Standards															
Dolomite-Ankerite															
12700	34	0.4961	0.0020	0.0003	0.5057	0.0018	0.0003	0.0009	0.0002	0.0000	0.0003	0.0002	0.0000	0.0024	0.0001
7920	36	0.4883	0.0026	0.0004	0.4985	0.0020	0.0003	0.0090	0.0007	0.0001	0.0011	0.0003	0.0001	0.0203	0.0003
6773	35	0.4825	0.0077	0.0013	0.4976	0.0068	0.0011	0.0145	0.0042	0.0007	0.0015	0.0004	0.0001	0.0321	0.0014
RK7	35	0.4778	0.0027	0.0005	0.4950	0.0024	0.0004	0.0157	0.0005	0.0001	0.0034	0.0002	0.0000	0.0384	0.0002
RK9	38	0.4689	0.0026	0.0004	0.4956	0.0021	0.0003	0.0248	0.0005	0.0001	0.0052	0.0006	0.0001	0.0601	0.0003
15086	29	0.3998	0.0114	0.0021	0.5018	0.0023	0.0004	0.0905	0.0109	0.0020	0.0021	0.0003	0.0001	0.1881	0.0043
Pulaski	68	0.2317	0.0081	0.0010	0.5094	0.0022	0.0003	0.2428	0.0068	0.0008	0.0135	0.0030	0.0004	0.5252	0.0023
16459	38	0.1833	0.0282	0.0046	0.5086	0.0033	0.0005	0.2946	0.0274	0.0044	0.0242	0.0025	0.0004	0.6349	0.0120
14102	25	0.1325	0.0035	0.0007	0.5224	0.0050	0.0010	0.3359	0.0054	0.0011	0.0242	0.0007	0.0001	0.7310	0.0029
Magnesite-siderite															
MRR 1077	12	0.9977	0.0039	0.0011	0.0029	0.0003	0.0001	0.0045	0.0005	0.0002	0.0010	0.0000	0.0000	0.0055	0.0002
2123	13	0.9954	0.0028	0.0008	0.0002	0.0004	0.0001	0.0055	0.0005	0.0001	0.0010	0.0000	0.0000	0.0064	0.0001
RK-6	22	0.9431	0.0052	0.0011	0.0029	0.0004	0.0001	0.0487	0.0015	0.0003	0.0069	0.0003	0.0001	0.0557	0.0003
SMS8	73	0.8678	0.0126	0.0015	0.0052	0.0007	0.0001	0.1181	0.0136	0.0016	0.0057	0.0015	0.0002	0.1248	0.0016
SMS9	94	0.6753	0.0176	0.0018	0.0056	0.0011	0.0001	0.2669	0.0022	0.0002	0.0530	0.0152	0.0016	0.3215	0.0018
9157	51	0.4996	0.0353	0.0049	0.0049	0.0021	0.0003	0.4908	0.0378	0.0053	0.0120	0.0009	0.0001	0.5016	0.0064
3247	29	0.3326	0.0255	0.0047	0.0067	0.0005	0.0001	0.6399	0.0268	0.0050	0.0305	0.0017	0.0003	0.6684	0.0068
10778	31	0.2048	0.0086	0.0015	0.0068	0.0028	0.0005	0.7600	0.0108	0.0019	0.0337	0.0062	0.0011	0.7949	0.0031
11734	29	0.1056	0.0149	0.0028	0.0080	0.0021	0.0004	0.8252	0.0152	0.0028	0.0707	0.0043	0.0008	0.8946	0.0046
3242	16	0.0025	0.0004	0.0001	0.0003	0.0003	0.0001	0.9607	0.0044	0.0011	0.0429	0.0014	0.0004	0.9975	0.0016
Calcite															
Cal_Opt	11	0.0043	0.0007	0.0002	1.0290	0.0039	0.0012	0.0002	0.0002	0.0001	0.0002	0.0001	0.0000		
Secondary Standards															

Chemically heterogeneous															
H884	*Chemically zoned, see Tables 7, 8*														
Chemically homogeneous															
RK-1 Magnesite	15	0.9232	0.0026	0.0007	0.0033	0.0223	0.0058	0.0488	0.0005	0.0001	0.0072	0.0002	0.0001	0.0572	0.0002
10937	26	0.1043	0.0054	0.0011	0.0151	0.0042	0.0008	0.8578	0.0064	0.0013	0.0359	0.0011	0.0002	0.8955	0.0020

Table 2: True isotopic composition of carbonate standards determined by bulk digestion techniques.

Name	(Fe+Mn)#	$\delta^{13}C$ (‰)	1SD	n	$\delta^{13}C$_conventional (‰)	1SD	n	$\delta^{26}Mg$ (‰)	1SD	n	$\delta^{44}Ca$ (‰)	1SD	n
Primary standards													
Dolomite-Ankerite													
12700	0.0024	0.06	0.12	3	0.04	0.06	3	-0.88	0.06	4	1.41	0.02	3
7920	0.0203	2.65	0.04	3	2.55	0.12	3	-0.90	0.05	4	0.69	0.02	3
6773	0.0321	-1.33	0.32	3	-1.27	0.08	3	-1.29	0.04	4	0.24	0.09	3
RK7	0.0384	-7.16	0.06	3				-0.87	0.05	3	0.46	0.19	3
RK9	0.0601	-7.38	0.25	2				-1.05	0.15	3	-0.03	0.06	3
15086	0.1881	-8.53	0.13	3	-8.58	0.01	1	-0.53	0.01	3	0.51	0.11	3
Pulaski	0.5252	-7.40	0.16	3	-7.35	0.50		-0.60		1	1.56	0.08	3
16459	0.6349	-5.57	0.25	2				0.54		1	0.36	0.01	2
14102	0.7310	-3.58	0.10	3				-1.05		1	0.58	0.10	3
Magnesite-siderite													
MRR 1077	0.0055	-0.95	0.01	3	-0.82			-1.14	0.06	2			
2123	0.0064	1.17	0.07	3				-1.02	0.04	6			
RK-6	0.0557	-6.02	0.19	3				-0.86	0.10	3			
SMS8	0.1248	-4.89	0.16	3				-0.61		1			
SMS9	0.3215	-9.71	0.03	2				-1.31		1			
9157	0.5016	-5.43	0.02	3				-0.47		1			
3247	0.6684	-6.37	0.03	3				-1.18		1			
10778	0.7949	-7.31	0.18	3	-7.27	0.03		-0.36		1			
11734	0.8946	-1.98	0.15	2									
3242	0.9975	-8.09	0.01	2									
Calcite													
Cal_Opt		2.78	0.02	3	2.69	0.03	2	-5.12	0.17	3	0.56	0.08	3
Secondary Standards													
Chemically heterogeneous													

H884		-8.26	0.28	2		-0.50	0.01	2	0.85	0.09	3
Chemically homogeneous											
RK-1 Magnesite	0.0572					-0.88	0.01	2			
10937	0.8955	-13.09	0.02	3							

Table 3: Secondary ^{12}C yield (cps/nA) and $^{13}IMF^*$ (relative to 7920 dolomite, ‰) for dolomite-ankerite, magnesite-siderite and calcite standards across two analytical sessions.

Name	(Fe+Mn)#	C isotope: Session 1					C isotope: Session 2				
		^{12}C yield (cps/nA)	1SD	n	$^{13}IMF^*$ (‰)	1SD	^{12}C yield (cps/nA)	1SD	n	$^{13}IMF^*$ (‰)	1SD
Dolomite-Ankerite					Rel 7920					Rel 7920	
12700	0.002	5.2E+05	5.5E+03	6	0.2	1.5	5.9E+05	3.0E+03	2		
7920	0.020	6.0E+05	4.9E+04	52	0.0	1.1	5.8E+05	3.0E+04	41	0.0	1.1
6773	0.032	5.7E+05	5.8E+03	3	-0.9	1.7	6.0E+05	5.2E+03	3	0.2	0.5
RK7	0.038	5.2E+05	5.8E+03	3			5.7E+05	4.3E+03	2		
RK9	0.060	5.4E+05	7.3E+04	8	-2.4	1.3	5.7E+05	1.5E+04	2	-1.8	1.2
15086	0.188	6.0E+05	5.7E+04	4	-4.9	0.5	6.3E+05	1.2E+04	8	-4.7	0.8
Pulaski	0.525	6.9E+05	1.7E+04	3	-1.5	1.1	7.9E+05	6.1E+03	4	-1.6	1.3
16459	0.635	7.1E+05	0.0E+00	2	-2.1	1.0	8.1E+05	2.2E+04	6	-1.2	1.4
14102	0.731	7.3E+05	1.7E+05	3	-1.7	1.3	8.3E+05	1.3E+04	6	-0.5	1.2
Magnesite-siderite											
MRR 1077	0.005	3.4E+05	5.8E+03	3	-2.2	2.0	3.6E+05	9.9E+02	3	-2.1	1.5
2123	0.006					-					
RK-6	0.056	4.1E+05	0.0E+00	2	-4.6	1.1	3.9E+05	8.5E+03	3	-3.7	1.0
SMS8	0.125	4.7E+05	5.8E+03	3	-7.4	1.6	4.4E+05	1.9E+03	5	-5.4	1.0
SMS9	0.321	5.2E+05	2.4E+04	4	-8.7	3.4	5.1E+05	3.2E+03	5	-5.9	1.0
9157	0.502	5.4E+05	0.0E+00	5	-7.9	1.8	5.2E+05	8.7E+03	3	-7.5	1.3
3247	0.668	5.3E+05	4.5E+03	5	-8.8	0.9	4.9E+05	1.3E+03	3	-7.8	1.0
10778	0.795	4.7E+05	2.1E+04	5	-7.7	1.5	4.4E+05	2.0E+04	3	-8.6	1.3
11734	0.895						3.7E+05	4.8E+03	4	-8.4	1.1
3242	0.998						2.4E+05	2.5E+03	4	-7.8	1.2

Calcite Cal_Opt			5.8E+05	8.1E+03	20	5.9	1.3

Table 4: Secondary ^{26,25}Mg yield (cps/nA) and ^{26,25}IMF* (‰) for dolomite-ankerite (relative to 12700 dolomite for session 1 mount 1 data and 7920 dolomite for all others), magnesite-siderite (relative to 2123 magnesite for session 1 and MRR1077 magnesite for session 2) and ^{26}IMF (absolute values, ‰) for calcite standards from two different mounts across two analytical sessions.

Name	(Fe+Mn)#	Mg isotope: Session 1, Mount1					Mg isotope: Session 1, Mount2					Mg isotope: Session 2						
		^{24}Mg yield (cps/nA)	1SD	n	^{26}IMF* (‰)	1SD	^{24}Mg yield (cps/nA)	1SD	n	^{26}IMF* (‰)	1SD	^{24}Mg yield (cps/nA)	1SD	n	^{26}IMF* (‰)	1SD	^{25}IMF* (‰)	1SD
Dolomite-Ankerite					Rel 12700					Rel 7920					Rel 7920		Rel 7920	
12700	0.002	2.4E+07	2.5E+05	4	0.0	0.5												
7920	0.020						2.6E+07	9.9E+04	6	0.0	0.3	2.8E+06	2.8E+05	11	0.0	0.3	0.0	0.6
6773	0.032						2.7E+07	5.4E+05	8	0.1	0.3							
RK7	0.038						2.7E+07	2.7E+05	7	0.3	0.2	2.7E+06	1.2E+04	3	1.0	0.5	0.6	0.2
RK9	0.060											2.7E+06	3.0E+04	3	2.0	0.3	1.6	0.0
15086	0.188	2.7E+07	1.2E+05	4	7.65	0.5	2.7E+07	2.3E+05	2	5.4	0.3	3.5E+06	3.0E+04	10	6.3	0.4	4.1	0.5
Pulaski	0.525	1.9E+07	1.3E+05	4	21.5	0.4	2.1E+07	2.1E+05	2	18.2	0.2	2.7E+06	7.8E+04	10	17.2	0.6	8.5	0.5
16459	0.635	1.8E+07	5.4E+05	4	23.8	0.6	1.9E+07	1.5E+05	2	20.0	0.3	2.1E+06	3.8E+04	3	19.6	0.1	10.5	0.2
14102	0.731	1.3E+07	3.0E+05	4	23.5	0.5	1.4E+07	1.1E+06	2	20.3	0.3	1.8E+06	3.5E+04	5	22.1	0.4	12.0	0.2
Magnesite-siderite					Rel 2123					Rel 2123					Rel MRR1077		Rel MRR1077	
MRR 1077	0.005											4.8E+06	7.1E+04	15	0.0	0.7	0.0	0.7
2123	0.006	1.3E+08	2.0E+07	25	0.0	0.2	1.4E+08	1.6E+07	44	0.0	0.3							
RK-6	0.056	1.5E+08	1.9E+07	5	8.0	0.2	1.2E+08	5.3E+05	3	7.6	0.2	5.3E+06	3.4E+04	4	3.7	0.4	1.8	0.5
SMS8	0.125	1.4E+08	8.0E+05	5	11.3	0.5	1.2E+08	5.2E+05	2	10.7	0.2	6.0E+06	8.8E+04	9	5.6	0.5	3.2	0.7
SMS9	0.321	1.3E+08	2.5E+06	4	10.9	0.3	1.2E+08	1.7E+05	2	11.5	0.4	5.4E+06	1.5E+04	4	13.8	0.2	7.9	0.4
9157	0.502	1.3E+08	1.1E+06	4	16.4	0.7	1.2E+08	1.5E+05	2	16.9	0.1	5.9E+06	2.4E+04	4	18.7	0.5	10.5	0.4

3247	0.668	1.1E+08	5.0E+05	4	17.6	0.3	1.4E+08	4.9E+05	2	18.2	0.3	4.7E+06	4.7E+04	4	20.1	0.5	10.8	0.4
10778	0.795	7.0E+07	7.0E+05	3	19.1	0.2	8.5E+07	4.8E+05	2	19.6	0.3	2.9E+06	6.6E+04	4	19.6	0.2	10.2	0.3
Calcite										Abs IMF								
Cal_Opt							1.2E+05	3.1E+03	22	-48.8	0.5							

Table 5: Secondary ^{40}Ca yield (cps/nA) and ^{44}IMF* (relative to 7920 dolomite, ‰) for dolomite-ankerite and calcite standards.

Name	Fe+Mn#	Ca isotope				
		^{40}Ca yield (cps/nA)	1SD	n	^{44}IMF* (‰)	1SD
Dolomite-Ankerite					Rel 7920	
12700	0.002					
7920	0.020	4.2E+06	8.9E+04	9	0.0	0.5
6773	0.032	4.4E+06	1.0E+05	8	0.6	0.8
RK7	0.038					
RK9	0.060					
15086	0.188	5.2E+06	4.0E+04	9	0.5	0.4
	0.188	5.2E+06	8.1E+03	2	0.5	0.5
Pulaski	0.525	6.7E+06	2.0E+05	8	0.5	0.4
16459	0.635	6.8E+06	9.8E+04	5	1.9	0.5
	0.635	6.7E+06	2.7E+05	3	2.6	0.3
14102	0.731	6.3E+06	2.9E+05	8	5.9	1.3
	0.731	6.3E+06	3.6E+05	13	5.6	1.5
Calcite						
Cal_Opt					-19.0	0.5
					-18.7	0.6

Table 6: Coefficients of polynomial fits to IMF*-(Fe+Mn)# data for different isotopic systematics from different analytical standards, where equation is of the form: $IMF^* = ax^4+bx^3+cx^2+dx+e$, where x = (Fe+Mn)#, along with regression R^2 values and calibration residuals (average and 1SD). Where sigmoidal functions are used to fit the IMF*-(Fe+Mn)#, the equation is of the form: $IMF^* = d+(a-d)/[1+(x/c)^b]$, where x = (Fe+Mn)#.

Analysis	IMF*	Session	Mineral series	Mount	Fitting function	Coefficients					R^2	Calibration redisuals	
						a	*b*	*c*	*d*	*e*		*Average*	*1SD*
C isotope	^{13}IMF* (‰)	1	Dol-Ank	2	Polynomial (3rd Order)		-111.770	147.130	-51.275	0.505	0.915	0	0.46
		1	Mgs-Sid	2	Polynomial (3rd Order)		-62.806	99.076	-46.344	-2.307	0.932	0	0.64
		2	Dol-Ank	2	Polynomial (3rd Order)		-108.230	152.610	-56.518	1.346	0.948	0	0.38
		2	Mgs-Sid	2	Polynomial (3rd Order)		-4.141	15.104	-16.370	-2.633	0.951	0	0.50
Mg isotope	^{26}IMF* (‰)	1	Dol-Ank	1	Polynomial (3rd Order)		-64.019	37.596	39.375	-0.132	0.999	0	0.42
		1	Mgs-Sid	1	Sigmoidal	-62.196	0.064	1.700E+10	385.650		0.998	0	0.35
		1	Dol-Ank	2	Polynomial (3rd Order)		-83.615	70.909	21.348	-0.568	1.000	0	0.12
		1	Mgs-Sid	2	Sigmoidal	-23.844	0.125	3.448E+10	947.662		1.000	0	0.20
	^{26}IMF* (‰)	2	Dol-Ank	2	Polynomial (3rd Order)		-1.150	-10.683	39.420	-0.600	1.000	0	0.20
		2	Mgs-Sid	2	Polynomial (3rd Order)		-21.121	-15.695	50.852	-0.345	1.000	0	0.14
	^{25}IMF* (‰)	2	Dol-Ank	2	Polynomial (3rd Order)		37.130	-47.514	32.186	0.493	0.999	0	0.19
		2	Mgs-Sid	2	Polynomial (3rd Order)		-12.910	-11.214	30.090	-0.242	0.999	0	0.13
Ca isotope	^{44}IMF* (‰)	1	Dol-Ank	2	Polynomial (4th Order)	86.647	-60.569	3.752	2.560	0.182	0.990	0	0.23
Fe isotope	56IMF* (1 nA)	1	Mgs-Sid	2	Polynomial (2nd Order)			57.183	-62.749	14.258	1.000	0	0.00
	56IMF* (reduced current)	2	Mgs-Sid	2	Polynomial (3rd Order)		-10.151	32.688	-28.587	-5.868	0.974	0	0.26

Table 7: Coupled major cation chemistry, secondary ^{12}C, ^{40}Ca yield (cps/nA) and $\delta^{13}C$, $\delta^{44}Ca$ (‰) of zoned secondary standard H884 and 10937, along with raw isotopic compositions measured by SIMS. Analytical uncertainties are 2SD (for $\delta^{13}C$) and 1SD (for $\delta^{44}Ca$) propagated.

Point	$MgCO_3$ (mol fraction)	$CaCO_3$ (mol fraction)	$SrCO_3$ (mol fraction)	$FeCO_3$ (mol fraction)	$MnCO_3$ (mol fraction)	(Fe+Mn)#	Carbon isotope				Calcium isotope			
							^{12}C yield (cps/nA)	Raw $\delta^{13}C$ (‰) (Drift corrected)	Corrected $\delta^{13}C$ (‰)	2SD	^{40}Ca yield (cps/nA)	Raw $\delta^{44}Ca$ (‰) (Drift corrected)	Corrected $\delta^{44}Ca$ (‰)	1SD
H884@1.asc	0.43	0.47	0.00	0.04	0.01	0.12	5.9E+05	-48.4	-3.8	2.3	5.0E+06	31.4	1.05	0.3
H884@2.asc	0.44	0.46	0.00	0.05	0.02	0.13	5.9E+05	-48.3	-3.4	2.3	5.2E+06	31.7	1.37	0.3
H884@3.asc	0.41	0.49	0.00	0.04	0.01	0.12	5.8E+05	-53.0	-8.5	2.7	5.4E+06	31.2	0.84	0.3
H884@4.asc	0.40	0.50	0.00	0.04	0.01	0.13	5.9E+05	-50.6	-5.9	2.3	5.4E+06	30.9	0.55	0.4
H884@5.asc	0.41	0.49	0.00	0.05	0.02	0.14	5.9E+05	-50.1	-5.1	2.8	5.4E+06	31.5	1.15	0.4
H884@6.asc	0.42	0.47	0.00	0.07	0.02	0.16	6.1E+05	-48.0	-2.6	2.6	5.5E+06	31.8	1.41	0.3
H884@7.asc	0.40	0.46	0.00	0.09	0.02	0.22	6.1E+05	-48.6	-2.8	2.2	5.7E+06	32.2	1.80	0.4
H884@8.asc	0.37	0.49	0.00	0.10	0.02	0.24	6.2E+05	-53.4	-7.8	2.7	5.9E+06	32.1	1.71	0.3
H884@9.asc	0.38	0.46	0.00	0.11	0.02	0.25	6.5E+05	-44.1	1.9	2.2	5.7E+06	31.5	1.18	0.3
H884@10.asc	0.35	0.49	0.00	0.11	0.02	0.28	6.3E+05	-50.1	-4.5	2.7	5.9E+06	31.0	0.69	0.3
H884@11.asc	0.35	0.49	0.00	0.11	0.01	0.26	6.2E+05	-47.0	-1.1	2.2	6.2E+06	31.4	1.03	0.3
H884@12.asc	0.34	0.49	0.00	0.12	0.01	0.29	6.4E+05	-51.3	-5.7	2.3	5.7E+06	31.2	0.89	0.3
H884@13.asc	0.36	0.48	0.00	0.11	0.02	0.26	6.3E+05	-48.9	-3.2	2.3	5.8E+06	31.1	0.77	0.3
H884@14.asc	0.37	0.47	0.00	0.11	0.02	0.25	6.2E+05	-51.2	-5.5	2.5	5.8E+06	31.1	0.75	0.3
H884@15.asc	0.30	0.52	0.00	0.12	0.03	0.33	6.3E+05	-48.6	-3.2	2.3	6.1E+06	30.6	0.37	0.3
H884@16.asc	0.38	0.48	0.00	0.09	0.02	0.23	6.1E+05	-52.9	-7.3	2.2	5.7E+06	30.9	0.49	0.3
H884@17.asc	0.42	0.47	0.00	0.06	0.02	0.16	6.0E+05	-55.1	-10.0	2.5	5.4E+06	31.2	0.76	0.3
H884@18.asc	0.42	0.48	0.00	0.06	0.02	0.15	5.9E+05	-51.7	-6.6	2.4	5.2E+06	32.7	2.29	0.3
H884@19.asc	0.41	0.50	0.00	0.04	0.02	0.13	5.8E+05	-56.3	-11.8	2.5	5.3E+06	30.1	-0.29	0.3
H884@20.asc	0.40	0.51	0.00	0.04	0.02	0.12	5.8E+05	-52.9	-8.4	2.3	5.2E+06	31.0	0.59	0.3
H884@21.asc	0.44	0.46	0.00	0.05	0.02	0.13	5.9E+05	-51.8	-7.2	2.2	5.1E+06	31.0	0.65	0.4
H884@22.asc	0.42	0.49	0.00	0.04	0.01	0.12	5.9E+05	-51.0	-6.4	2.1	5.4E+06	31.0	0.63	0.3
H884@25.asc	0.37	0.51	0.00	0.07	0.02	0.20	5.9E+05	-58.1	-12.8	2.4	5.6E+06	29.6	-0.84	0.3
H884@26.asc	0.35	0.51	0.00	0.09	0.02	0.23	6.2E+05	-54.3	-8.7	2.2	5.8E+06	30.3	-0.11	0.4
H884@27.asc	0.35	0.51	0.00	0.09	0.02	0.24	6.2E+05	-51.3	-5.6	2.6	5.8E+06	30.3	-0.10	0.3

H884@28.asc	0.35	0.51	0.00	0.09	0.02	0.24	6.3E+05	-53.3	-7.7	2.2	6.0E+06	29.8	-0.54	0.3
H884@29.asc	0.35	0.50	0.00	0.10	0.02	0.25	6.2E+05	-52.6	-7.0	2.4	5.8E+06	30.2	-0.15	0.3
H884@30.asc	0.36	0.51	0.00	0.09	0.02	0.23	6.3E+05	-54.0	-8.5	2.3	6.0E+06	30.5	0.14	0.3
H884@31.asc	0.36	0.51	0.00	0.09	0.02	0.23	6.2E+05	-55.9	-10.4	2.5	5.9E+06	30.6	0.15	0.4
									SIMS grain average	**2SE**			**SIMS grain average**	**2SE**
									-6.2	1.2			0.66	0.3
10937@1.asc	0.10	0.02	0.00	0.86	0.04	0.90	3.2E+05	-58.0	-15.4	2.9				
10937@2.asc	0.10	0.02	0.00	0.86	0.04	0.90	3.2E+05	-55.8	-13.3	2.4				
10937@1.asc	0.10	0.02	0.00	0.86	0.04	0.90	3.2E+05	-56.8	-14.3	3.0				
10937@2.asc	0.10	0.02	0.00	0.86	0.04	0.90	3.2E+05	-55.1	-12.6	2.6				
10937@3.asc	0.10	0.02	0.00	0.86	0.04	0.90	3.2E+05	-56.8	-14.3	2.4				
10937@4.asc	0.10	0.02	0.00	0.86	0.04	0.90	3.2E+05	-55.8	-13.3	2.5				
10937@5.asc	0.10	0.02	0.00	0.86	0.04	0.90	3.2E+05	-54.9	-12.4	2.7				
10937@6.asc	0.10	0.02	0.00	0.86	0.04	0.90	3.1E+05	-56.3	-13.8	2.5				
10937@7.asc	0.10	0.02	0.00	0.86	0.04	0.90	3.2E+05	-56.2	-13.7	2.6				
10937@8.asc	0.10	0.02	0.00	0.86	0.04	0.90	3.3E+05	-55.3	-12.8	2.5				
10937@9.asc	0.10	0.02	0.00	0.86	0.04	0.90	3.1E+05	-53.2	-10.7	3.2				
10937@10.asc	0.10	0.02	0.00	0.86	0.04	0.90	3.1E+05	-56.5	-14.0	2.6				
10937@11.asc	0.10	0.02	0.00	0.86	0.04	0.90	3.1E+05	-55.3	-12.8	2.6				
10937@12.asc	0.10	0.02	0.00	0.86	0.04	0.90	3.1E+05	-56.9	-14.4	2.9				
10937@13.asc	0.10	0.02	0.00	0.86	0.04	0.90	3.1E+05	-56.1	-13.6	2.8				
10937@14.asc	0.10	0.02	0.00	0.86	0.04	0.90	3.2E+05	-54.9	-12.4	2.2				
10937@15.asc	0.10	0.02	0.00	0.86	0.04	0.90	3.1E+05	-54.5	-12.0	2.9				
10937@16.asc	0.10	0.02	0.00	0.86	0.04	0.90	3.1E+05	-53.8	-11.3	2.2				
10937@17.asc	0.10	0.02	0.00	0.86	0.04	0.90	3.2E+05	-53.5	-11.0	2.4				
10937@18.asc	0.10	0.02	0.00	0.86	0.04	0.90	3.1E+05	-55.9	-13.4	2.7				
10937@19.asc	0.10	0.02	0.00	0.86	0.04	0.90	3.0E+05	-53.4	-10.9	2.8				
10937@20.asc	0.10	0.02	0.00	0.86	0.04	0.90	3.1E+05	-54.3	-11.8	2.6				

SIMS grain average	2SE
-13.9	0.6

Table 8: Major cation chemistry, secondary ^{26}Mg yield (cps/nA) and $\delta^{26}Mg$ (‰) of zoned secondary standard H884 (from two different mounts) and magnesites RK-1 and MRR1077 (treated as secondary standard), along with raw isotopic compositions measured by SIMS. Analytical uncertainties are 1SD propagated.

Point	^{24}Mg yield (cps/nA)	$MgCO_3$ (mol fraction)	$CaCO_3$ (mol fraction)	$SrCO_3$ (mol fraction)	$FeCO_3$ (mol fraction)	$MnCO_3$ (mol fraction)	(Fe+Mn)#	Raw $\delta^{26}Mg$ (‰) (Drift corrected)	Corrected $\delta^{26}Mg$ (‰)	1SD
Master2_H884@1.asc	2.560E+07	0.36	0.52	0.00	0.07	0.02	0.20	-46.4	-0.36	0.2
Master2_H884@2.asc	2.551E+07	0.36	0.51	0.00	0.08	0.02	0.22	-45.4	-0.02	0.2
Master2_H884@3.asc	2.643E+07	0.36	0.51	0.00	0.08	0.02	0.22	-47.1	-1.78	0.2
Master2_H884@4.asc	2.611E+07	0.35	0.50	0.00	0.10	0.02	0.25	-44.2	-0.01	0.2
Master2_H884@5.asc	2.763E+07	0.42	0.49	0.00	0.04	0.01	0.12	-49.5	-0.67	0.3
Master2_H884@6.asc	2.710E+07	0.43	0.48	0.00	0.05	0.02	0.13	-49.8	-1.02	0.3
Master2_H884@7.asc	2.844E+07	0.41	0.49	0.00	0.05	0.02	0.13	-49.0	-0.52	0.3
Master2_H884@8.asc	2.599E+07	0.41	0.49	0.00	0.05	0.02	0.13	-49.5	-1.09	0.3
Master2_H884@9.asc	2.982E+07	0.42	0.47	0.00	0.07	0.02	0.17	-47.8	-0.45	0.3
Master2_H884@10.asc	2.793E+07	0.38	0.48	0.00	0.09	0.02	0.23	-43.9	1.03	0.3
Master2_H884@11.asc	2.992E+07	0.37	0.47	0.00	0.10	0.02	0.25	-43.5	0.79	0.3
Master2_H884@12.asc	2.863E+07	0.36	0.48	0.00	0.11	0.02	0.27	-42.0	1.52	0.3
Master2_H884@14.asc	2.552E+07	0.36	0.51	0.00	0.09	0.02	0.23	-45.2	-0.35	0.3
									Mount 2 average	2SE
									-0.22	0.5
CompactH884@1.asc	2.411E+07	0.38	0.51	0.00	0.07	0.02	0.18	-48.7	-0.83	0.4
CompactH884@2.asc	2.427E+07	0.38	0.51	0.00	0.06	0.02	0.17	-48.3	-0.17	0.4
CompactH884@3.asc	2.403E+07	0.38	0.51	0.00	0.06	0.02	0.17	-48.7	-0.62	0.5
CompactH884@4.asc	2.381E+07	0.38	0.51	0.00	0.06	0.02	0.17	-49.1	-1.03	0.4
CompactH884@5.asc	1.953E+07	0.38	0.51	0.00	0.06	0.02	0.18	-47.6	0.39	0.5

CompactH884@6.asc	1.955E+07	0.38	0.51	0.00	0.06	0.02	0.18	-47.5	0.49	0.5
CompactH884@7.asc	1.953E+07	0.38	0.51	0.00	0.06	0.02	0.16	-48.0	0.65	0.5
									Mount 1 average	2SE
									-0.16	0.5
									SIMS grain average	**2SE**
									-0.20	0.4
Master2_MRR1077@1.asc	1.051E+08	0.92	0.00	0.00	0.05	0.01	0.06	-49.0	-1.20	0.3
Master2_MRR1077@2.asc	1.050E+08	0.92	0.00	0.00	0.05	0.01	0.06	-48.7	-0.95	0.3
Master2_MRR1077@3.asc	1.057E+08	0.92	0.00	0.00	0.05	0.01	0.06	-49.3	-1.54	0.3
									SIMS grain average	**2SE**
									-1.23	0.3
RK_1_mgs@1.asc	1.561E+08	0.92	0.00	0.00	0.05	0.01	0.06	-40.2	-1.18	0.27
RK_1_mgs@2.asc	1.552E+08	0.92	0.00	0.00	0.05	0.01	0.06	-40.3	-1.26	0.26
RK_1_mgs@3.asc	1.546E+08	0.92	0.00	0.00	0.05	0.01	0.06	-40.2	-1.20	0.27
									SIMS grain average	**2SE**
									-1.21	0.05

View Article Online
DOI: 10.1039/D6JA00136J

Data availability

All data supporting this article are present in the paper and/or the Supplementary Information.